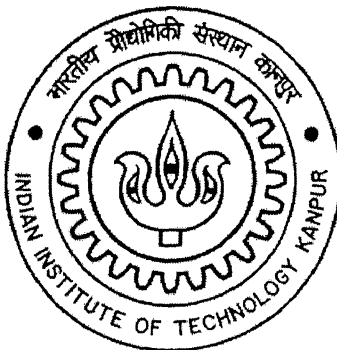# SPARK PLASMA SINTERING AND CHARACTERIZATION OF TITANIUM DI-BORIDE BASED COMPOSITES

A THESIS SUBMITTED

IN PARTIAL FULFILMENT OF THE REQUIREMENTS FOR THE MASTER OF TECHNOLOGY DEGREE
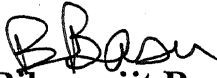
By

T. VENKATESWARAN

ROLL NO. Y220621

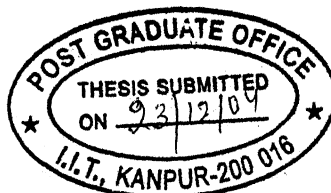*Thesis Supervisor: Dr.Bikramjit Basu*

TO THE

DEPARTMENT OF MATERIALS AND METALLURGICAL ENGINEERING

.INDIAN INSTITUTE OF TECHNOLOGY – KANPUR

January 2005

CERTIFICATE

This is to certify that the work contained in the thesis entitled *"Spark Plasma Sintering and Characterization of Titanium di-boride Based composites,"* by **T. Venkateswaran** (Roll No. **Y220621**) has been carried out under my supervision and to the best of my knowledge this has not been submitted elsewhere for a degree.

Dr. Bikramjit Basu
Assistant Professor
IIT- Kanpur

POST GRADUATE OFFICE
THESIS SUBMITTED
ON 23|12|04
I.I.T., KANPUR-200 016

Acknowledgments

Research Publications:

Publications arising from this thesis:

1) **T. Venkateswaran**, B. Basu, DY Kim, "Spark Plasma Sintering of TiB_2-based composite materials", communicated to J. Am. Cer. Soc., December 2004.

2) **T. Venkateswaran**, B. Basu, DY Kim, "Processing and Characterization of Transition metal borides-based cermets via Spark Plasma Sintering", communicated to J. Eur. Ceram. Soc., December 2004.

Other publications:

3) **T. Venkateswaran**, D. Sarkar and B. Basu, "Understanding the wear properties of WC-ZrO_2 Nanocomposites", J. Am. Cer. Soc. (in Press, 2004).

4) B. Basu, **T. Venkateswaran** and D. Sarkar, "Pressureless sintering and Tribological properties of WC-ZrO_2 composites", J. Eur. Cer. Soc. (in Press, 2004).

5) **T. Venkateswaran**, D. Sarkar and B. Basu, "WC-ZrO_2 Composites: Processing and Unlubricated Tribological Properties", Wear (in Press 2004).

6) **T. Venkateswaran**, B. Basu, DY Kim, "Spark Plasma Sintering and Characterization of ZrO_2-ZrB_2 nanoceramic composites", communicated to J. Am. Cer. Soc., December 2004.

7) **T. Venkateswaran**, S. Bhodak, K-H Jung, W. Joo, B. Basu, D-Y Kim, "Fretting wear behavior of (W,Ti)C-Co cermets", (under preparation).

CONTENTS

Abstract

TiB_2-based materials received wider attention in materials science community because of high melting point, low density, high hardness, wear resistance. However poor densification and moderate fracture toughness restricts their wider application. The densification of TiB_2 has been a major problem due to strong covalent bonding, low self-diffusion coefficient and the existence of oxygen rich surface layer on the particle surface. The appropriate selection of binder (type and amount) and the processing parameters is required to obtain dense borides. In the present work, the sintering of monolithic TiB_2, TiB_2 with 10 wt% of $MoSi_2$ and TiB_2 with 6 wt. % Cu addition are carried out using Spark Plasma Sintering (SPS) technique. SPS experiments are carried out in the temperature range of 1200-1500°C under vacuum with a heating rate of 500-600K/min and the optimization of the SPS conditions is established. The enhanced sintering of monolithic TiB_2 to full density at lower temperature (1400°C) ensures the grain boundary cleaning and enables binderless sintering in SPS route. Furthermore, the synergetic effect of sintering aid ($MoSi_2$) as well as SPS processing route enhanced the densification of TiB_2 composites at the lower temperature (1400-1500°C) in shorter time (10-15 min). Additionally detailed microstructural analysis of the SPS processed sample is carried out using XRD and SEM in order to understand the detailed densification mechanism. The mechanical and electrical properties of the developed TiB_2 composite are also evaluated. The SPSed $TiB_2/MoSi_2$ composite is characterized by high hardness of ~18 GPa and moderate indentation toughness of ~ 5 MPa m$^{1/2}$. Also $TiB_2/MoSi_2$ composite exhibits better electrical conductivity value (~0.08-0.09 $M\Omega^{-1} .cm^{-1}$), when compared with both monolithic TiB_2 (0.07 $M\Omega^{-1} .cm^{-1}$) and $MoSi_2$ (0.05 $M\Omega^{-1} .cm^{-1}$). The optimized TiB_2/Cu cermet exhibits hardness and fracture toughness of ~17 GPa and ~11 MPa m$^{1/2}$. High electrical conductivity of ~ 0.20 $M\Omega^{-1}. cm^{-1}$ (TiB_2/Cu) is also measured with the optimized cermets.

Key words: TiB_2, $MoSi_2$, Cu, Spark Plasma Sintering.

List of Figures:

List of Tables:

List of Symbols:

T_m - Melting point [K].

ω - Maximum possible evaporation rate.

ρ_s - Density of the material (gm/cc)

J - Accommodated current density (A m^{-2}).

M   - Atomic weight.

p - Saturation pressure of the metal vapor.

p_l - Actual vapor pressure.

D_{50} - Median particle diameter (μm).

H_v - Vickers hardness (GPa).

K_{Ic} - Fracture toughness (MPa m$^{1/2}$).

E   - Elastic modulus (GPa).

2c   - Radial crack length from enumerated from Vickers indentation (μm).

ρ - Electrical resistivity (μΩ. cm).

$1/\rho$ - Electrical conductivity (MΩ^{-1}. cm^{-1}).

Chapter 1

Introduction
- Spark Plasma Sintering

1. Spark Plasma Sintering (SPS)

1.1 Introduction

Sintering commonly refers to processes involving heat treatment of powder compacts at elevated temperatures, usually at $T>0.5$ T_m [in Kelvin], i.e. in the temperature range where diffusional mass transport is appreciable. Successful sintering usually results in a dense polycrystalline solid. Several variables influence the rate of sintering, among that the principal variables that control shrinkage at all stages of sintering includes: temperature, time, pressures, particle size, chemical composition of starting powder mixture, and the sintering environment. The geometric progression associated with the sintering can be divided into three stages. During the initial stage, bonds form at the particle contacts. The physics of the process involved with intermediate stage of sintering are: a) neck growth, b) pores forming arrays of interconnected cylindrical channels and c) particle centers approaching one another, resulting in compact shrinkage. The isolation of pores, elimination of porosity and grain growth are the characteristic features associated with the final stage of sintering, leading to densification more than 93% ρ_{th}. The stages of sintering represent a change in driving force for mass flow at high temperatures. The initial strain after compaction can leads to a plastic flow contribution to sintering, but generally diffusive processes are dominant. The possible diffusion paths include lattice, grain boundary and surface regions. There is a characteristic distinction between surface and bulk diffusion process. Bulk transport provides densification, while surface transport causes interparticle bonding without densification. Overall, sintering can be broadly classified into a) solid state sintering, b) liquid phase sintering and c) viscous sintering. While solid state sintering solely depends on the above diffusional transport processes,

the liquid phase sintering (LPS) involves the enhanced mass transport in the presence of a wetting liquid, which forms at or near the sintering temperature. Viscous sintering, similar to LPS, is a dominant densification mechanism for silica based traditional ceramics, which are not the focus of the present study. LPS is an attractive option for many of the high performance materials like TiB_2, because of faster densification at lower temperature and better combination of obtainable mechanical properties. To enhance the overall process, external pressure or chemical additives needs to be used. Now-a-days, versatile advanced sintering technologies have also been developed for successful densification of ceramic/metallic materials with better properties enhancement. The prominent among them are Microwave Sintering, Spark Plasma Sintering, Laser Sintering etc.

Among wider categories of advanced sintering technology, the Spark Plasma Sintering (SPS) belongs to the family of activated sintering techniques and is also a widely used technique in recent times. Activated sintering which lowers the activation energy, allows the densification to occur at lower sintering temperature, shorter sintering time with better properties. Activated sintering is accompanied with increasing driving force through the following ways,

1) Pressure assisted activation

2) Chemical activation by the addition of second phase through chemical reaction

3) Physical activation i.e application of electric current

To obtain fully dense component, the densification must often be enhanced by adopting appropriate concepts, as described above. External pressure normally contributes to the

driving force. The pressure applied during the heating process helps in attaining maximum densification faster, when compared to pressureless sintering process. A chemical reaction, as a result of addition of sintering activators, provides additional driving force during sintering. The chemical reaction usually provides much more driving force when compared with pressure assisted driving force. Criteria to be fulfilled for an effective additive are the formation of low melting species during sintering and large solubility in base metals. Formation of segregated layer provides a high diffusivity path for rapid sintering to occur. The kinetics of activated sintering through additives addition depends on rate of diffusion through the activators. In some instances, the role of activators is to remove surface oxide from the powder particle surface or to facilitate more rapid diffusion. The minor additives can influence many factors such as interfacial energies, diffusion coefficients, grain boundary mobility and grain boundary phase distribution, however their role is not clear.

In SPS process, the rapid densification of metal and ceramic powders are achieved by the application of current during the sintering process, which result in the physical activation of the powder particle surface during sintering and hence enhance the densification through surface and grain boundary diffusion. All the sintering activation methods, discussed above, attempt to lower the activation barrier for the densification by altering either kinetics or driving force accompanied with sintering phenomena [1-3].

The following sections focus on the densification enhancement through application of current, characterized feature of the equipment widely called as "Spark Plasma Sintering (SPS)".The way it differs from conventional Hot Pressing (HP) is application of current in addition to the application of pressure. As a result of enhanced activated sintering,

maximum densification without exaggerated grain growth is obtained in the final sintered component [4].

Section 1.2 explains the various driving force accompanied with the sintering of SPS. Section 1.3 provides brief ideas of the history of development of SPS and various nomenclatures practiced for SPS instrument. The details of the instrumentation were explained in the section 1.4. The mechanism of the SPS is explained in section 1.5. Section 1.6 discusses the serious problem of temperature profile associated with SPS. Advantages of SPS is pointed clearly in the section 1.7. Section 1.8 discusses various research centered with SPS processing techniques i.e. sintering of nanomaterials and various other advanced materials. This will be followed by short concluding remarks of the SPS in section 1.9

1.2. Driving forces assisting plasma sintering

Sintering is accompanied by the lowering of free energy of the system. The sources which give rises to this lowering of free energy are called as driving force for the sintering. Fig.1.1 demonstrates the various driving forces associated with spark plasma sintering. Three major sources contributing to the densification in SPS processes include:

1) Resistance heating or Joules Heating

2) Pressure application

3) Surface activation of the powder particle surface

These three sources provide unique contribution to the lowering of free energy of the during sintering and makes it different form other conventional joules heating sintering techniques. The surface activation due to electric current application is quite special and

makes the SPS process a distinct one. This current application results in the cleaning of the grain surfaces, helps in direct grain to grain contact and causes enhanced grain boundary diffusion. All these help in achieving full densification of the powder compact [4-9].
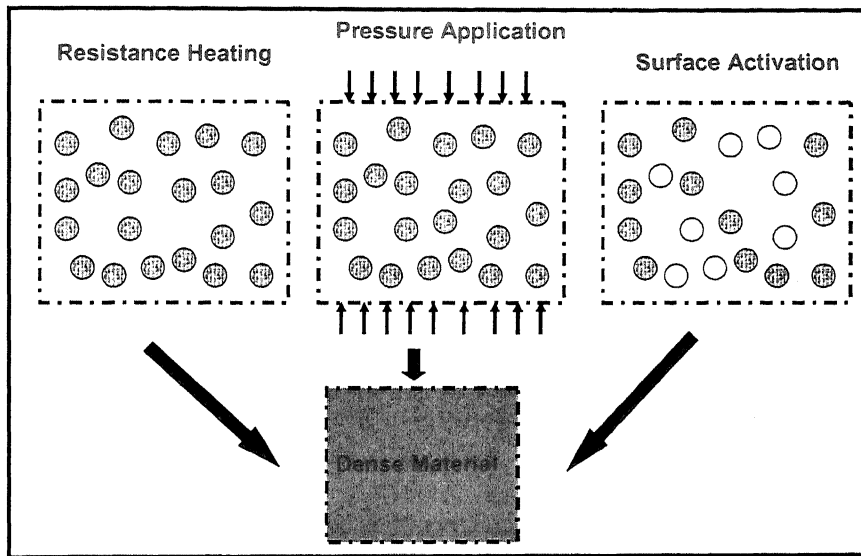
Fig.1.1 The driving forces associated with the Spark plasma Sintering.

1.3. Chronicle of SPS

Until now versatile Field Activated Sintering Techniques (FAST) have been developed, based on the application of pressure and electric current application. Taylor in 1933 established a process associated with the application of pressure during sintering and he used cemented carbides for his investigation. Following Taylor, Cremer in 1944 claimed a patent for the field-assisted Sintering. The material used for the investigations are pure Cu and Cu-alloys, pure Al and parameters used for consolidation include: current ~ 60 Hz for 1to 2 cycles, current density ~ 62 kA/cm^2, pressure ~ 70-140 MPa. Following the

pioneering work, the research in this area was triggered and later in 1950's, sintering of metal powders are carried out with the equipment similar to spot welding.

Another variation of FAST includes powder compaction due to pinch effect, arising from magnetic forces induced by large electric current. These include dynamic magnetic compaction (DMC) and indirect high-energy high-rate processing (HEHR). The concentration of pulse electric current in the compaction zone, give arise to magnetic filed forces, which in turn leads to pressure increment of around 5 GPa. In electro discharge compaction (EDC), a variation of activated sintering techniques, the initial powder activation is carried out by the application of pulses. The main difference of EDC with FAST is number of pulse applied. FAST is characterized by continuous current application. While in EDC, a current is applied for the initial activation of the powder particle surfaces.

The continuous application of electric current through the sintering period, leads to sustained activation of the powder particle surfaces and hence triggers the sintering to occur in shorter time. In last few decades, SPS received the attention of the researchers in the materials community and various companies started production of this instrumentation throughout the world with variation in nomenclature. Commercially available nomenclature of plasma sintering are plasma activated sintering (PAS, Japan), instrumented pulse-electro discharge consolidation or spark sintering under pressure (Korea), pulsed electrical discharge with pressure application (Russia) and Plasma pressure consolidation (USA). The main concepts behind all the instruments are same, i.e. the mechanism is based on pressure and electric current application. An essential identification parameter of the FAST is certainly the electric current application [4-9].

1.4. Instrumentation and Operation

The schematic of the Spark Plasma Sintering unit is shown in Figure 1.2. The two major components of the SPS unit are 1) the mechanical component, that supplies required pressure during consolidation and 2) the electrical devices for the application of pulsed and steady electric current. There is no need of prior cold compaction, loose powders are loaded directly into the graphite mold and proper insulation with graphite sheet or BN spray is used in the internal diameter of the graphite to avoid contamination at higher temperature. The advantages behind loading loose powders, improves the current path through the powders and facilitate better densification. It is well known that the electrical conductivity of the graphite with loose powders is much higher than that of the compacted one. The use of graphite put limitation of the pressure applied and it varies with size of the graphite die used. For 10 mm internal diameter (punches diameter~10 mm), the maximum pressure is limited bellow 50 MPa. Moreover the graphite provides a reducing environment. The chamber as well as the ram / electrode transferring pressure are water-cooled. The equipment is attached with linear gauge for measuring the shrinkage during the sintering process. There is a facility for controlled atmosphere also. Initially the pulsed discharge is achieved by the application of high voltage followed by the application of current. The conductive powders are mainly heated due to joules effect. For non-conductive powders, heating occurs by the transfer of heat from the die and punches [6].
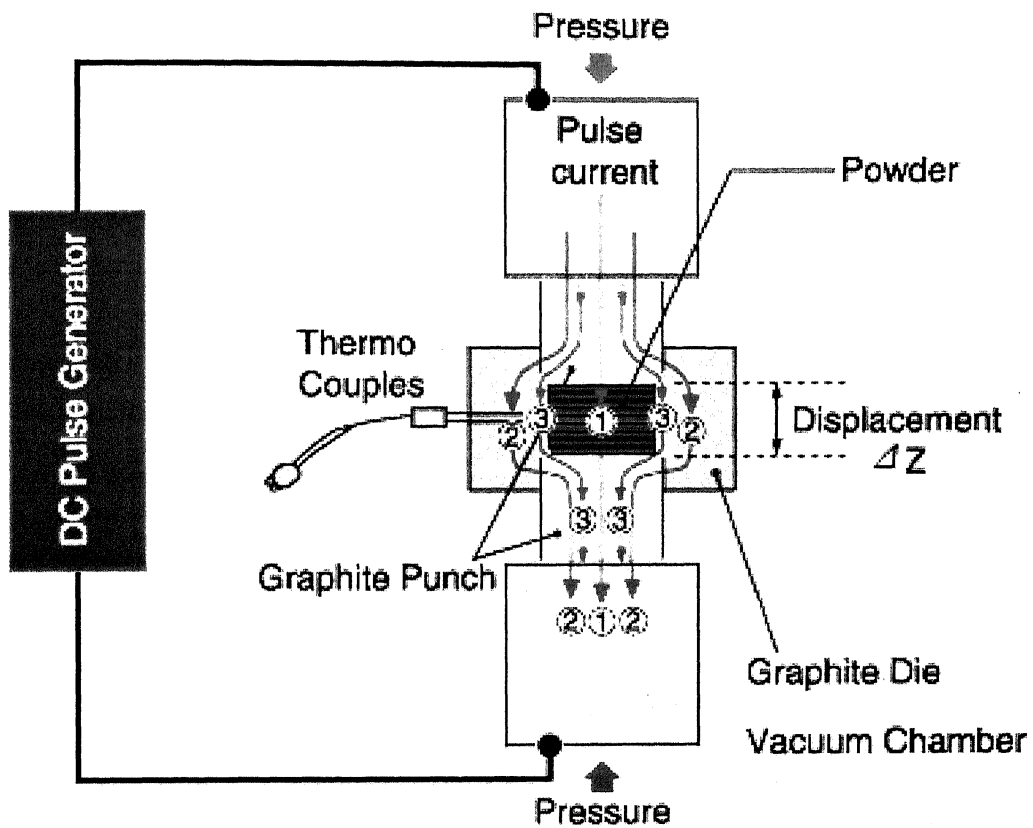
Fig.1.2 Schematic of the Spark Plasma Sintering (SPS) unit revealing various mandatory components.

1.5. Consolidation Mechanism

During SPS process, it is assumed that the small capacitors are formed at particle contacts i.e (a) in insulating surface films at the contact between particles and (b) in the gap around the particle contact. The electrical discharges are generated across these capacitor gaps. The interfering surface oxide films are pierced when a certain voltage level is achieved, depending on the dielectric strength of the oxide layer. The mechanisms of electrical failure takes place, when the breakdown voltage is reached and this involves arcing across adjacent points on particles and electrical breakdown of dielectric film on the powder particle surface. Alternatively, the electrical discharges around the contacts may generate plasma, i.e an ionized gas between the powder particles. These phenomena collectively contribute to the physical activation of the powder particle surface. The physical activation combined with faster densification at lower temperatures reduces grain coarsening and preserves a finer microstructure in the sintered material. The SPS mechanism broadly depicted in the Fig. 1.4.

SPS sintering temperatures range from low to over 2000°C and maximum densification is usually achieved at temperature 200°C to 500°C lower than that of conventional sintering. Vaporization, melting and sintering are completed in short periods of approximately 5 to 20 minutes, including temperature rise and holding times. The mechanism involving the spark discharge appears in the gap between the particles of a material and leads to a high local temperature. This causes vaporization and the melting of the surfaces of the powder particles during the SPS process. The constricted shapes or "necks" are formed around the contact area between the particles. These necks gradually develop and neck growth progresses during sintering, resulting in a sintered compact of over 99% density. Since

only the surface temperature of the particles rises rapidly by self-heating, growth of the starting powder materials is controlled. Therefore, a precision sintered compact is manufactured in a shorter time. Spark Plasma Sintering results in accelerated densification with minimum grain coarsening, while achieving a good metallurgical grain-to-grain bonding. The later may be partly explained by the ability to remove the oxides and impurities from the particle surfaces. Like in the present case, TiO_2 surface oxide layer on TiB_2 is successfully removed either by mechanical removal of the surface oxides or by physical activation of the powder particle surface prior to the densification. In field activated sintering, oxide removal and subsequent good interparticle bonding may be attributed to phenomena ranging from resistance heating to thermal and electrical breakdown of insulating films and discharge or arching. As in any sintering process field activated densification starts with a highly porous body. The initial pressure application proceeds with neck formation. The neck formation is due to the geometric amplification of the pressure on the interparticle point contacts, but as the necks grow the local pressure at the necks is substantially reduced. At this stage the pulsed current is applied and a current path is established in metal or conductive ceramic powders. The goal is to achieve a uniform current path rather than local channels that may concentrate all passing current (Fig 1.3). Usually, the initial 1-2 pulse applications ensure uniform current path, particularly for high resistance powders. Next the current is forced to choose the path contact points to complete the current path through powders. An important phenomenon associated with arching is material transfer that results in physical mechanism for charge transport along the gap. This is accomplished by vaporization of the surface of the material. When the pressure is high, vapor is vigorously produced from the surface

together with fine liquid droplets from the contact. It is conceivable that some surface cleaning from oxides and impurities take place during this process. This vapor can lead to intermittent plasma formation. An estimate of the maximum possible evaporation rate is given by,

$$\omega = \frac{440}{\rho_s \, J} \sqrt{\frac{\overline{M}}{T}} (p - p_1)$$

Where ρ_s is the density of the material, J is the accommodated current density (A m^{-2}), M is the atomic weight, T is the temperature, p is the saturation pressure of the metal vapor and p_1 is the actual vapor pressure. [4]

Beyond the electrical discharge stage, the sintering parameters in FAST have a similar effect as in conventional pressure sintering. After the particles have been connected together, the second stage starts when a direct current is applied. Diffusion process and plastic flow are the main contributors to the densification in this stage. The highest temperatures achieved in the necks provide the highest diffusion rates and thus enhanced matter transport towards the neck area. [4-9].
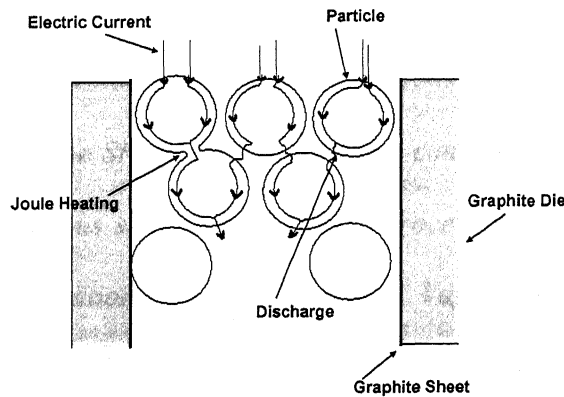
Fig. 1.3. Schematic of the current path through the powders loaded in the graphite die and associated phenomenon.
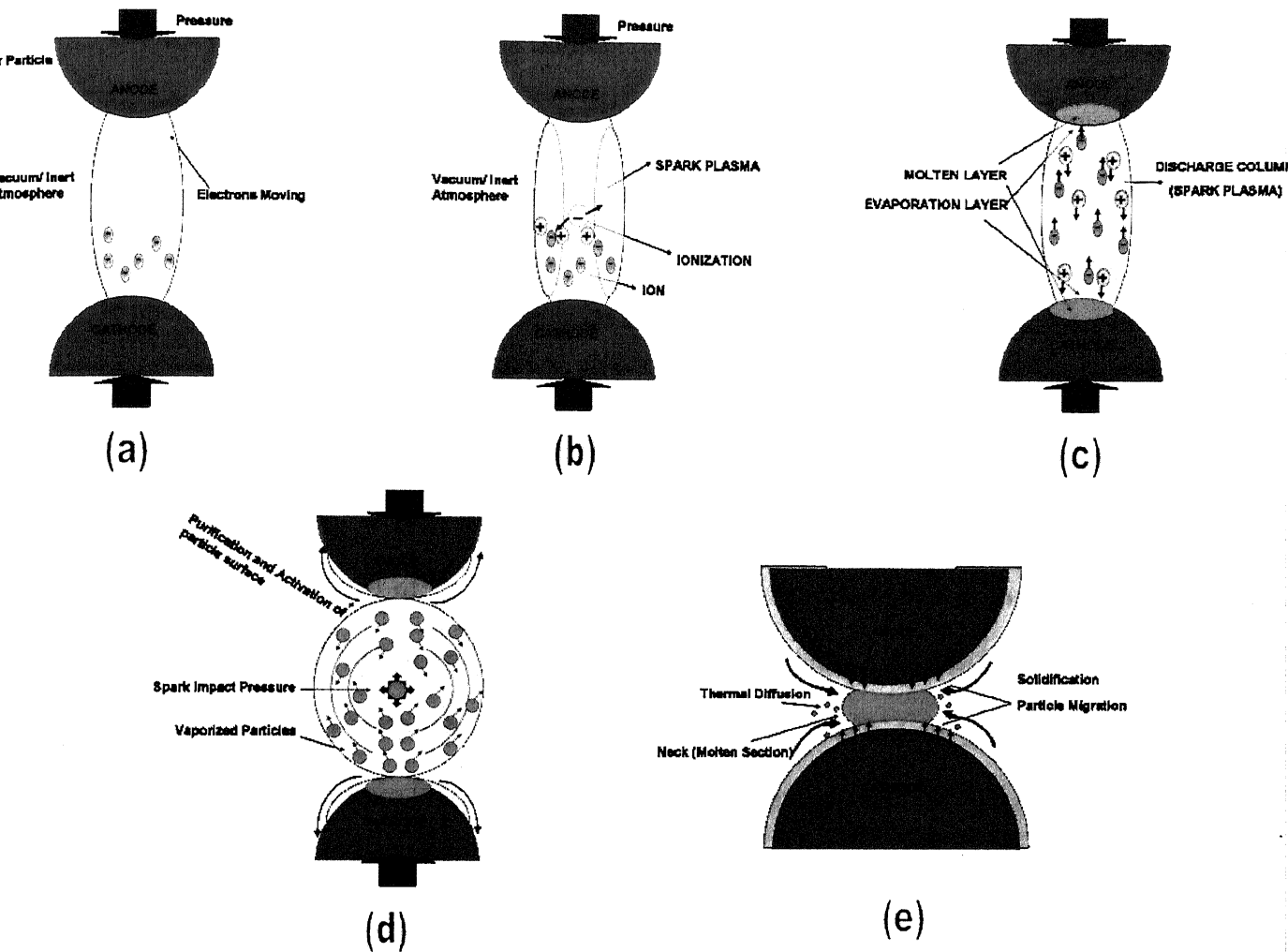
Fig.1.4. Schematic of the SPS mechanisms, which contribute to the consolidation of the powder particles. Various steps involved in the process includes; Initial stage of Spark Discharging (a), Generation of Spark Plasma (b), Vaporization and Melting of powder particle surface (c), Generation of powder spark impact pressure, Sputtering of vaporized / molten particles (d) and Neck formation by Spark Plasma.

1.6. Temperature profile associated with SPS

The temperature field distribution during sintering becomes an important consideration because of the high heating rate involved with SPS processing. The temperature difference of 130°C was observed from the center of the sample to the inner surface of the die during the consolidation Ni powders consolidation [10]. However, the temperature gradient critically depends on the thermal conductivity of the material to be sintered, graphite die etc. Therefore it is important to find out the theoretical model to compare temperature gradient distribution [10]. The experiments conducted on the TiB_2 and BN shows that, at final holding temperature, the temperature difference of around 450°C from the centre of the sample to the outside of the sample was measured [10] using thermouple inserted appropriately (Fig. 1.5). The higher the conductivity of the sample, smaller the temperature differences from inside to outside of the sample. The difference in temperature is also directly related with heating rate. This difference can be minimized if proper insulation actions are taken accordingly.

Moreover, the temperature is measured from the outside of the chamber using the optical pyrometer port that focused towards the graphite die assembly, which always results in error in assessing the real sample temperature. Similarly, the temperature gradient also varies for conducting and non-conducting powders and more complex in the case of the composite powders. Therefore, there should be a trade off between the measured temperature and the real temperature of the sample. More research in this direction is required to evaluate the temperature profile in SPS process. In our present investigation, as mentioned in the instrumentation section, the temperature profile relation between the

graphite die and sample inside are correlated prior to the experiments with thermocouple appropriately inserted in the graphite mold.
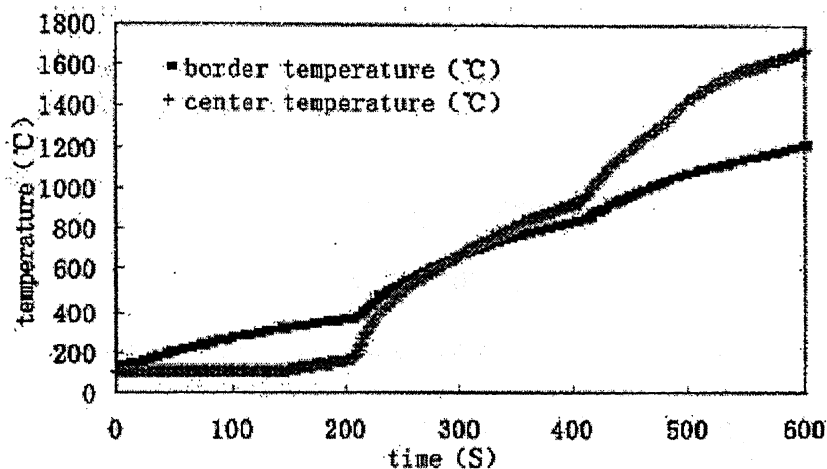
Fig. 1.5 True temperature rising curve as measured with SPS process [10].

1.7. Advantages of SPS

As a beginning of new era in sintering technology, Spark Plasma Sintering provides tremendous advantages over the other conventional sintering, developed until now. The specific advantages of SPS are as follows [4-10]:

a) The rapid rate of densification (heating rate upto 600-500K/min) and achieving full density in shorter time

b) Removal of the need for cold isostatic pressing

c) Elimination of additive use and debinding

d) Microstructural refinement upon solidification leading to increase in steel hardenability and enhancing sintering and machining processes

e) Consolidation of difficult-to-sinter powders

f) Higher sintered density at lower temperatures

9) Finer microstructure and better mechanical properties.

1.8. Literature Review

1.8.1. SPS of Nanomaterials:

In recent times, nanoceramics and nanoceramic composites have received wider attention among the materials science community because of the expectation that nanocomposite ceramics can exhibit improved mechanical properties, wear resistance, chemical inertness, corrosion resistance and thermal insulating properties. [11–16]. Ceramic nanocomposites were first developed in Japan, mainly by K. Niihara claiming that ceramic materials with excellent mechanical properties can be obtained through nanocomposite technology [17]. According to Niihara, nanocomposites are materials fabricated by dispersion of nanosized particles within micron-sized matrix grains or at the grain boundaries of the matrix, where as nano-nanocomposites are formed when matrix grains are also in the nanosize scale. The processing of nanoceramics inevitably demands the adoption of a specific processing route, which would restrict grain growth while achieving full densification. This has particularly become feasible with the use of field activated sintering technique (FAST). FAST involves the imposition of an electrical field during sintering. SPS is one of the widely used FAST techniques. A considerable part of recent research on the development of several structural nanocomposites using SPS techniques have been reported in the literature [18-20].

Gao and co-workers reported a significant increase in strength (over 1 GPa) and fracture toughness (from 3.25 to 4.70 MPa.m$^{1/2}$) as resulted from addition of 5 wt. % SiC nanoparticles to a micron sized Al_2O_3-15 wt. % ZrO_2 (3Y) matrix [18]. High hardness of 17 GPa is measured in dense Al_2O_3 - 5 wt. % SiC- 15 wt. % ZrO_2 (3Y) materials after spark plasma sintering (SPS) at 1450°C with a heating rate of 600^{0}C/min and without any

holding at sintering temperature. Perara et al. had reported faster densification of Si_3N_4/SiC composites using the SPS route and also compared to that obtained by sinter/hot isostatic pressing (HIP) route [19]. Fully dense Si_3N_4 composites were fabricated by SPS processing at 1900^0C with dwell time of 5 minutes. Recent research carried out by Gao et al. had indicated that SiC-mullite nanocomposites with full density could be processed via SPS route at a relatively lower temperature of 1500^0C [20]. These nanocomposites with 5-10 vol % SiC addition exhibit moderate strength of around 400-500 MPa. However, the fracture toughness remains low and around 2 MPa m$^{1/2}$.

1.8.2. Role of SPS in densification of other advanced materials

Laboratory scale FAST experiments have been performed for a large variety of materials ranging form metals to intermetallics compounds to ceramics and composites. Sintering of AlN had been successfully carried out using SPS at 1727°C for a holding period of 5 min, without any sintering addition. The conventional sintering of AlN route requires temperature of 1927°C with a prolonged holding period of 30h [21]. Successful densification of the $MoSi_2$ with relative density of 97% have been achieved at SPS temperature of 1700°C in vacuum [22]. Moreover, oxidation behavior in the accelerated oxidation temperature region of $MoSi_2$ showed that accelerated oxidation was remarkably suppressed for SPSed $MoSi_2$. The densification result and hardness of SPSed $MoSi_2$ are much better than that of hot pressed samples. Functionally graded materials such as ZrO_2 on NiCrAlY and TiAl have been consolidated to high densities through SPS processing [23]. The observation of clean grain boundaries (HRTEM results) of tungsten sintered at

2327°C to a density of 91.5% in 8 min, indicates the grain boundary cleaning mechanism associated with SPS [24].

It is well established that sintering of WC compacts is difficult in conventional sintering without sintering addition and hence sintering can be aided with secondary binder phases of Co, Fe and Ni. WC-Co cemented carbide is valuable for use in cutting tools and dies. But pure WC powders can be consolidated successfully in the SPS at the temperature range above 1700°C [25]. The unreinforced WC is an excellent ceramic with applications as tool and machine parts. Different superconductors like YBCO and MgB_2 have been successfully sintered to full densification via SPS [26]. An increase in T_c temperature with SPSed YBCO from 240 to 278K was recorded. Also, a sharp superconducting transition with an onset temperature of 38.5K was measured with spark plasma sintered MgB_2 [27]. For the first time, WC-6 wt. % ZrO_2 nanocomposites with full density is obtained using the SPS route at relatively lower sintering temperature of 1300°C (5 min). SPS route showed clear superiority in terms of achieving faster densification of WC – ZrO_2 composites compared to that obtained by pressureless sintering route (1700^{0}C, 1h). Remarkably high hardness of 23-24 GPa is achieved in dense SPS-processed WC composites [28]. The dense microstructure, characterized by submicron WC particles and nano-ZrO_2 reinforcement, is observed to be responsible for high hardness. Despite high hardness, the newly developed WC-based composites exhibited rather moderate toughness of around 6 MPa m$^{1/2}$. Different Y-stabilization (3, 2, 0 mol %) does not seem to have any noticeable influence as far as the toughness concerned. At present, research is going on in exploiting use of SPS in ceramic – ceramic joining and ceramic – metal joining [29].

1.9. Outlook

SPS has enabled significant improvements in the synthesis and processing of new advanced materials, especially in the following four areas (1) sintering technology for rapid, grain boundary controlled and temperature gradient sintering, (2) bonding technology for bonding dissimilar/similar, graded and solid-solid materials, (3) surface treatment technology for the modification and surface hardening of plasma spray coated layers and (4) synthesis technology for solidification of polymers, growth of single crystals, synthesis of eutectic substances and other processes. Spark plasma sintering (SPS), characterized with certain inherent advantages like high-thermo efficiency, quick heating schedule, helps in faster sintering under low temperature and better self-purification of the surface of the powder particle. A strong enough electrical field is produced in the small gaps of the particles to make the electrons, cations and anions to strike the surface of the opposite particle and purify it surfaces. Thus SPS is efficient in achieving densification of a wide spectrum of materials and in particular, difficult to sinter powders. The nanomaterials are enjoying the advantage of rapid heating of powder particle surface and densification without much exaggerated grain growth. The process is also amenable for mass production. Some of the important issues that need to be elucidated with SPS include a scientifically accepted mechanism for densification associated with SPS chamber and temperature profile during spark plasma sintering. Additionally issues like the role of SPS on liquid phase sintering, grain growth, mechanical and functional properties need to be investigated by careful design of SPS experiments on some model materials systems.

1.10 Reference:

[1] R. M. German and Z. A. Munir, "Activated Sintering of Refractory Metals by transition Metal Additions", Rev. Powder Met. Phys. Ceramics, 2 9-43 (1982).

[2] R. M. German, "Powder Metallurgy Science", Metal powder Industries Federation, Princeton, New Jersey, USA.

[3] M. N. Rahaman, "Ceramic Processing and Sintering", Marcel Dekker, Inc. New York.

[4] J. R. Groza, A. Zavalianges, Sintering Activation by external electric field, Mat. Sci. and Engg., A287 171-177 (2000).

[5] S. W. Wang, L. D. Chen and T. Hirai; Densification of Al_2O_3 powder using spark plasma sintering; J. Mat. Res., 15 [4] 982 (2000).

[6] B. Basu, J. H. Lee and D. Y. Kim, "Development of Nanocrystalline wear resistant Y-TZP ceramics", J. Am. Cer. Soc., 87 [9] 1771-1774 (2004).

[7] L. Gao, H. Z. Wang, J. S. Hong, H. Miyamoto, K. Miyamoto, Y. Nishikawa and S. D. D. L. Torre, Mechanical properties and microstructure of nano-SiC-Al_2O_3 composites densified by Spark Plasma Sintering, J. Eur. Cer. Soc., 19 609-613 (1999).

[8] D. S. Perara, M. Tokita and S. Moricca; Comparative study of Fabrication of Si_3N_4/ SiC composites by Spark Plasma Sintering and Hot Isostatic Pressing, J. Eur. Cer Soc., 18 401-404 (1998).

[9] Lian Gao, Xihai Jin, Hirokazu Kawaoka, Tohru Sekino and Koichi Niihara; Microstructure and mechanical properties of SiC- mullite nano composite prepared by spark plasma sintering, Materials Science and Engineering., A334, 262-266 (2002).

[10] Wang Yucheng and Fu Zhengyi, Study of temperature field in spark plasma sintering, Materials Science and Engineering B90 34 - 37 (2002).

[11] M. Sternitzke; Review: Structural Ceramic Nanocomposites, J. Eur. Cer.Soc.,17, 1061-1082, (1997).

[12] R. D. Shull; View Point: nanocrystalline and nano phase materials, Nano Structured Materials 2 213-216 (1993).

[13] R. S. Averbek, H. J. Holfer, and R. Tao; Processing of nano-grained materials, Materials Science and Engineering A66 169-177 (1993).

[14] S. Komarneni; Nanocomposites, J. Mater. Chem., 2 [12] 1219-1230 (1992).

[15] C. Suryanarayana; Nanocrystalline Materials, International Materials Reviews, 40, 41-64 (1995).

[16] H. Gleiter; Nanostructured Materials: state of the art and perspectives, Z. Metallkd., 86 78-83 (1995).

[17] K. Niihara; New design concept of structural ceramics-ceramic nano composites, J. Ceram. Soc. Jap., The Centennial Memorial Issue., 99[10] 974-982 (1991).

[18] L. Gao, H. Z. Wang, J. S. Hong, H. Miyamoto, K. Miyamoto, Y. Nishikawa and S. D. D. L. Torre; Mechanical properties and microstructure of nano-SiC-Al$_2$O$_3$ composites densified by Spark Plasma Sintering, J. Eur. Cer. Soc., 19 609-613 (1999).

[19] D. S. Perara, M. Tokita and S. Moricca; Comparative study of Fabrication of Si$_3$N$_4$/ SiC composites by Spark Plasma Sintering and Hot Isostatic Pressing, J. Eur. Cer Soc., 18 401-404 (1998).

[20] Lian Gao, Xihai Jin, Hirokazu Kawaoka, Tohru Sekino and Koichi Niihara; Microstructure and mechanical properties of SiC- mullite nano composite prepared by spark plasma sintering, Materials Science and Engineering., A334 262-266 (2002).

[21] S.H. Risbud, J.R. Groza, M.J. Kim, Phil. Mag. 69 525 (1994).

[22] I.J. Shon, Z. A. Munir, K. Yamazaki and K. Shoda, Simultaneous Synthesis and Densification of MoSi$_2$ by field actvated combustion, J. Am. Ceram. Soc., 79 [7] 1875-1880 (1996).

[23] S.K. Hur, S. H. Yoo, J.R. Groza, J.M. Doh, K. Yamazaki and K. Shoda, Graded coatings by gradient temeperature densification. J. Mater. Res., May 1998.

[24] T.J. Goodwin, S.H. Yoo, P. Matteazzi, J.R. Groza, Nanostructure. Mater. 8 559 (1997).

[25] S.I. Cha, S.H. Hong, Microstructure of binderless tungsten carbides sintered by Spark Plasma Sintering Process, Mat. Sc and Engg., A356 381-389 (2003).

[26] S. H. Riabud and C-H Shan, Resistivity Drops at >240 K and diamagnetic AC susceptibility up to 300 K in Rapidly Consolidated YBCO, Matter. Lett., 20 149-153 (1994).

[27] SY Lee, SI Yoo, YW Kim, N. M. Hwang and DY Kim, "Preparation of Dense MgB2 bulk superconductors by Spark Plasma Sintering", J. Am. Ceram. Soc., 86 [10] 1800 -1802 (2003).

[28] T. Venkateswaran, D. Sarkar and B. Basu; Understanding the wear properties of WC-ZrO$_2$ Nanocomposites; J. Am. Cer. Soc. (in Press, 2004).

[29] S. Yoo, J.R. Groza, T.S. Sudarshan and K. Yamazaki, Diffusion Bonding of BN on Metal Substrates by Plasma Activated Sintering (PAS) process, Scr. Mater., 34 [9] 1383-1386 (1996).

Chapter 2

Literature Review
- TiB$_2$ based materials

2. TiB$_2$ based materials

2.1 Introduction

The attractive combination of hardness, thermal and electrical properties of TiB$_2$ based materials made them suitable for various engineering applications, such as cathode material for hall heroult cell, aluminum evaporation boat, Electro Discharge Machining (EDM) electrode, armour material, conductive coating and wear components [1-4]. Because of strong covalent bonding, high melting point and relatively low self-diffusion coefficient, the densification of monolithic Titanium di-boride (TiB$_2$) is needed to be carried out at relatively high sintering temperature (>1800°C) and longer holding time (> 1hr) in conventional pressureless sintering route [5-8]. Moreover, internal stresses as a consequence of grain growth at higher sintering temperature triggers microcracking, resulting in degradation of mechanical properties [9, 10]. Until now research efforts are focused on obtaining densification of TiB$_2$ based materials at lower temperature using metallic as well as ceramic binders [11,12]. However, the addition of various metallic binders are detrimental for high temperature applications. In last few decades, extensive research efforts focused towards the addition of the optimized amount of metallic binder in order to enhance densification by forming amorphous or crystalline reaction products in liquid Phase Sintering (LPS) route. However, metallic binders often form complex borides with boron oxide and free boron, resulting in insufficient wetting of TiB$_2$ grains and hence increase sintering temperature [13].

Alternatively, the use of ceramic binders is also explored in achieving maximum densification with better properties [11, 14-16]. The major motivation behind the addition of binders is to eliminate the oxide layer from the TiB$_2$ particle surface and results in the

formation of amorphous or crystalline phase during sintering. The elimination of oxide layer can be achieved in two ways: a) by addition of sintering additives, b) by high temperature sintering to evaporate oxygen rich species (TiO_2). Various reaction products e.g. SiO_2, $(Ti, Zr)_5Si_3$, $(Ti, Zr)B_2$, $(Ti, Ta)B_2$ are reported to be formed with addition of various sintering additives like SiC, ZrO_2, TaC, TaN respectively to TiB_2 base material [17-19]. Also, another group of researchers used reaction sintering and mechanochemical processing route to obtain TiB_2-based composite with better densification and mechanical properties [20, 21].

In this investigation, $MoSi_2$ is selected as a one of the sintering additive for TiB_2 material. $MoSi_2$, an intermetallic compound, is a candidate material for high temperature applications and often used as heating elements, aircraft components, turbine blades etc [22,23]. Optimized amount of $MoSi_2$ addition to TiB_2 can potentially lead to the development of particulate reinforced ceramic-ceramic composite with improved thermal and electrical properties for high temperature application. In a recent work, we reported the microstructure and properties of TiB_2-$MoSi_2$ materials, processed via hot pressing route [24]. It was observed that full densification and better mechanical properties can be obtained after hot pressing at 1700°C for 1 hr with 10 wt. % $MoSi_2$ addition. Following this, the present work is taken up to investigate the densification and property study using SPS as a processing tool. Now-a-days Spark Plasma Sintering (SPS) is widely used for faster sintering of nanomaterials as well as various structural materials [25-27]. The major advantage of SPS includes faster densification at lower sintering temperature and shorter holding time without exaggerated grain growth. The present investigation will explore the synergetic effect of addition of sinter-additive ($MoSi_2$) and SPS processing

route on the densification and properties of TiB$_2$-based materials. In the second part of the present investigation, the densification study on the TiB$_2$ is conducted in the presence of the metallic binder addition (Cu) in aiming towards a) densification b) toughness increment and c) electrical property enhancement. 6 wt. % Cu is added to TiB$_2$ as sinter-additives.

2.2 Phase diagram and crystal structure

It is observed from the Ti-B binary phase diagram that the TiB$_2$ phase is most stable upto high temperature (see Fig. 2.1). In Ti-B binary system, three intermetallic phases, e.g. orthorhombic TiB, orthorhombic Ti$_3$B$_4$ and hexagonal TiB$_2$ can be formed. While TiB and Ti$_3$B$_4$ decompose peritectically at 2180°C and 2200^{0}C, respectively, TiB$_2$ melts congruently at ~3225^{0}C. Both TiB and TiB$_2$ phases have a narrow homogeneity range, whereas Ti$_3$B$_4$ has a fixed composition. TiB$_2$ exists over a stoichiometry range of 28.5-30 wt% B. Due to its stability and high melting point, TiB$_2$ is considered as an important candidate material for high temperature structural applications. In TiB$_2$, the Ti atoms form a hexagonal close packed (HCP) structure. The hexagonal unit cell of single crystal TiB$_2$, having space group P6/mmm [a=b=3.029A^0, c=3.229A^0; $\alpha=\beta=90^0$, $\gamma=120^0$] is shown in Fig. 2.2(a). Ti atoms are located at (0, 0, 0) and B atoms at (1/3, 2/3, 1/2) and (2/3, 1/3, 1/2) lattice sites. In analogy with the usual notation of ABABAB for HCP, the stacking sequence of Ti will be AAA. The boron B atoms are situated interstitially between the A-layers forming a strong covalently bonded hexagonal network structure (see Fig. 2.2b). The high hardness and Young's modulus of TiB$_2$ as well as its chemical resistance are attributed to the inherent crystal structure and atomic bonding (covalent).

Some important physical and mechanical properties of TiB_2 are presented in Table 2.1. When compared to the most commonly used hard materials, TiB_2 (33.38 GPa) is harder than TiC (31.52 GPa), WC (23.29 GPa) and TiN (19.80 GPa) [28]. Despite having useful properties, the applications of monolithic TiB_2 is rather limited due to poor sinterability, exaggerated grain growth and poor oxidation resistance. To overcome this problem, various metallic and non-metallic binders are used to obtain dense borides. Since densification has been a major challenge to obtain dense borides, the sintering of borides will be discussed in detail.
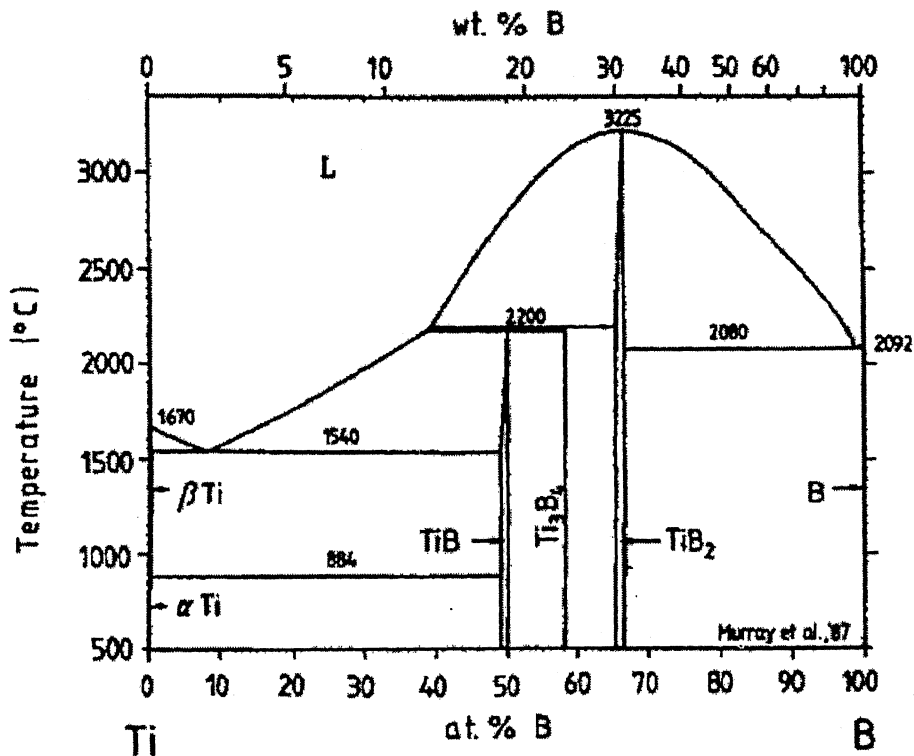
Fig. 2.1 Ti-B binary phase diagram [29, 30]
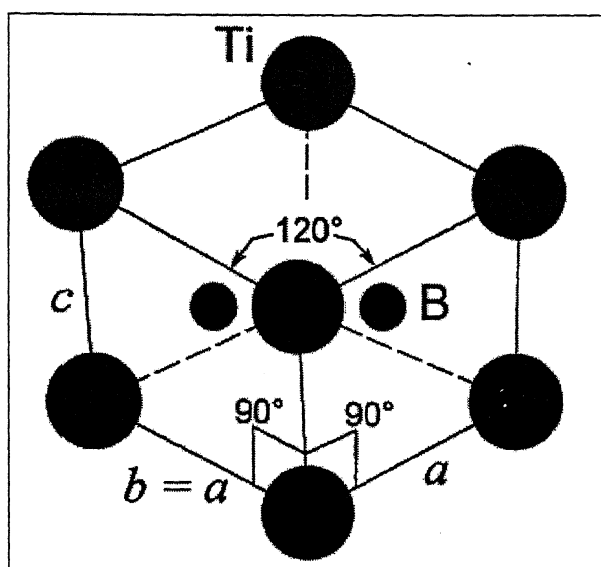
(a)
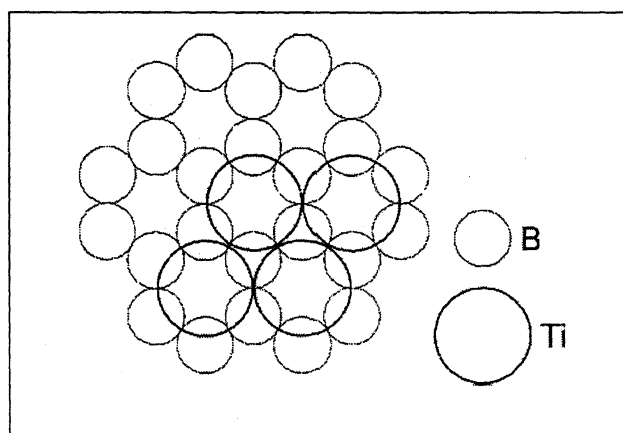
(b)

Fig. 2.2 The hexagonal unit cell of single crystal TiB₂, $a = b \neq c$, [a=b=3.029A⁰; c=3.229A⁰], $\alpha = \beta = 90^0$, $\gamma=120^0$ and the location of Ti at (0,0,0), B at (1/3,2/3,1/2) and (2/3,1/3,1/2) (a) and illustration of the hexagonal net of boron atoms, the Ti are situated half c-axis above and below the boron network. The c-axis is perpendicular to the paper (b) [29, 30].

26

Table 2.1 Summary of important physical and mechanical Properties of TiB₂

Property	TiB$_2$
Melting Point (^{o}C)	3200
Thermal conductivity (W/m/K)	60 – 120
Density (g/cc)	4.52
Coefficient of linear expansion (^{o}C^{-1})	8.1 X 10^{-6}
Electrical resistivity ($\mu\Omega$. cm)	10 – 30
Fracture toughness K$_{IC}$ (MPa.m$^{1/2}$)	5 – 7
Hardness (G Pa)	32
Elastic modulus (G Pa)	~500
Oxidation Resistance in air	up to1000^{o}C
Friction coefficient (self mated)	0.9
Specific heat (J/Kg/K)	617

2.3 Use of metallic binders in densification

Extensive research has reported the role of metallic binders on the densification and properties of TiB$_2$. Earlier sintering experiments using metallic additives like such as nickel, iron, cobalt, stainless steel, and manganese have demonstrated that 99% ρ_{th} can be achieved by liquid phase sintering (LPS). Ferber et. al. used up to 10 wt% Ni to achieve more than 99% theoretical density by hot pressing route (1400^{0}C) [7]. As

far as the densification mechanism is concerned, the transition metals (Ni, Co, Cr) react with TiB_2 forming various metal borides with a low melting point (~ 900^0C -1100^0C) and these borides also exhibit good wetting behavior. In the case of Ni-bonded TiB_2, a ternary τ-phase with the composition, $Ni_{21}Ti_2B_6$ forms by the dissolution of TiB_2. At 800^0C, the τ-phase is in equilibrium with Ni, Ni_3B, Ni_3Ti, and TiB_2. Typical metal contents required for the optimum liquid phase sintering of TiB_2 are 5 to 25 wt. % (2 to 12 at. %) of either Ni or Co. In order to avoid reactions consuming TiB_2, the borides of Ni or Co have also been used [31]. In LPS route, the sintering temperatures have been decreased from 2100^0C to 1400^0C. The liquid phase intensifies the mass transport, but causes accelerated grain growth. However, extensive nickel phase transformation was found to have deleterious effect on both fracture strength and fracture toughness. However, the strength and toughness are significantly enhanced for TiB_2 ceramics with a fine grain size (4 μm) and modest Ni content (<2 wt %).

Kang et al [12] have observed that simultaneous addition of 0.5 wt. % Fe and 0.5 wt. % Cr enhances the densification of TiB_2 in the temperature range of $1800-1900^0C$. They have shown that when small amount of Fe (0.5 wt %) is added, abnormal grain growth occurs and hence lowering the sintered. In case of B_4C addition along with 0.5 wt % Fe, abnormal grain growth was suppressed remarkably and there was an increase in sintered density up to 95% ρ_{th}. Microstructural observation confirmed the existence of Fe-rich phase at the triple junction and at grain boundaries. The microstructures of the TiB_2 composites prepared by liquid phase sintering are similar to those of other hard metals like WC-Co. The TiB_2 particles form a rigid skeleton of faceted crystals, whereas the binder forms compounds of Fe, Cr, or Co e.g., Ni_3B, Ni_2B, Ni_3B_4. Depending upon

the wetting behavior, typically influenced by the surface oxidation of the hard phase, round pores may accumulate at particle/matrix interfaces or close to triple junctions, which can not be completely infiltrated by the liquid phase. Moreover, the evaporation of Fe-, Co-, or Ni- borides may cause entrapped gas pores. Hence, hot-pressing is required for a homogeneous distribution of the liquid phase, particle rearrangement, and complete removal of the residual porosity. In contrast to hard metals based on Co, the matrix phase is very brittle, e.g., the K_{Ic} of Ni$_3$B equals 1.4 –1.9 MPa m$^{1/2}$ [31], and hence does not improve the mechanical properties.

The fabrication of TiB$_2$ based cermets, resembling the well-known WC-Co hard metal, combines the high toughness and ductility of a metallic binder with the hardness of the boride phase. This is recently achieved by using Fe instead of Ni and Co [31]. Although there are still some controversies concerning the phase diagram of Ti-B-Fe, TiB$_2$ is in a eutectic equilibrium with liquid Fe at 1340^{0}C (eutectic concentration 6.3 mol% TiB$_2$), which enables liquid phase sintering. Discrepancies exist for the phase equilibria at lower temperatures because of the problem of whether the observed Fe$_2$B is an equilibrium phase or results from impurities present in the staring powders. It is, however, obvious that oxygen and carbon contaminants, introduced during the powder synthesis routes significantly affect the wetting behavior of the liquid Fe. Both constituents do indeed cause dramatic changes in the phase equilibria and sintering kinetics, and thus have to be compensated for by the addition of metallic Ti, Mo or Nd to form TiC, or Ti$_2$O$_3$ and Nd$_2$O$_3$, respectively, to act as a carbon or oxygen trap [31].

Since the eutectic concentration in the quasi-binary TiB$_2$-Fe system with 14 vol.% TiB$_2$ is considerably closer to the metal-rich side than in the similar WC-Co system

(32 vol.% WC), a much smaller amount of liquid phase is generated upon sintering which makes densification more difficult [31]. A simple increase in temperature cannot satisfactorily balance the lack of liquid, because it is accompanied by accelerated coarsening of TiB_2 due to Oswald ripening. The volume fraction of binder phase thus ranges between 10 and 30%. A typical microstructure is very similar, as TiB_2 particles are embedded in a continuous Fe matrix like that of WC-Co hard metals. The densification mechanisms are typically dissolution-reprecipitation as well as coalescence, i.e., rearrangement and intergrowth of particles with common faces of the same orientation. The latter mechanism is active if the volume fraction of liquid exceeds 30%, but may result in the growth of elongated platelets. The residual porosity after pressureless sintering at 1500-1800^{0}C depends upon the initial liquid phase composition. At 1500^{0}C, 88% ρ_{th} of the theoretical density has been obtained for the TiB_2-Fe system (99% ρ_{th} at 1800^{0}C); whereas at 1450^{0}C, Ti addition results in 98% theoretical density and combined Ti-Nb additives result in 96.7% theoretical density. Hot pressing and hot isostatic pressing can yield densities > 98% with a lower binder content [31].

Pressureless sintering of titanium diboride with nickel, nickel boride and iron additives has also been experimented. Einarsrud and co-workers [6] reported the effect of relatively small additions (1–5 wt %) of nickel, nickel boride (NiB), and iron to promote the liquid-phase sintering of titanium diboride (TiB_2). Carbon was also added to some samples, in order to reduce the amount of oxygen impurities in the TiB_2 ceramics. The green bodies, formed by uniaxial pressing were sintered in a graphite furnace at 1300-1700^{0}C, both under vacuum and in a 500 mbar argon atmosphere. High densities (>94% ρ_{th}) were obtained at temperatures greater than or equal to 1500^{0}C. The weight loss of the

samples during sintering was shown to be dependent on the densification rate and the final density was not governed solely by the thermodynamics of the system. Significant exaggerated grain growth was observed in samples with binders like nickel, NiB, and iron during sintering at 1700^0C. The exaggerated grain growth was observed to be closely related to the oxygen content of the samples and sintering temperature. The addition of carbon strongly reduced the density and the oxygen content and, thereby, inhibiting the grain growth. They have proposed that exaggerated grain growth is enhanced by surface diffusion in a titanium-oxide-rich layer on the TiB_2 grains. The rate of exaggerated grain growth (or the number of large grains) in the system was decreased by a) lowering the sintering temperature, b) adding 1.5 wt% of iron instead of 1.5 wt% nickel, c) performing the sintering under vacuum instead of in an argon atmosphere, and d) decreasing the nickel content from 5 wt % to 1.5 wt%. Also, the exaggerated grain growth seems to have a correlation with the weight loss or the secondary phase. Einarsrud and co workers [6] proposed that the exaggerated grain growth in TiB_2 ceramics is enhanced by oxygen impurities. For the samples with added carbon in addition to nickel, the grain growth was inhibited (under vacuum)/limited (in an argon atmosphere), and these samples were shown to contain small amounts of oxygen. However, because the density of these samples was quite low, exaggerated grain growth was not expected to occur. Baik and Becher [32] have noted the importance of oxygen as an active species to increase surface diffusion and grain growth during the pressureless sintering of TiB_2.

Kang and Kim [12] reported the pressureless sintering and properties of titanium diboride ceramic containing chromium and iron. Simultaneous addition of 0.5 wt. % Cr and Fe was found to enhance the densification of TiB_2. The densities of specimens that were

sintered for 2h at 1800^0C and 1900^0C were 97.6% and 98.8% of the theoretical density respectively. The mechanical properties of the specimen sintered at 1800^0C, (strength of 506 MPa and a fracture toughness of 6.16 MPa.m$^{1/2}$), were much better than those observed in the specimen sintered at 1900^0C.

2.4 Use of non-metallic additives in densification

It is now recognized that, the presence of metallic binder was not desirable for high temperature structural applications as the low melting point of metallic elements leads to incipient fusion and consequently the degradation in the properties. Therefore, non-metallic additives should be preferred with an aim to improve sinterability without promoting grain growth and also to retain high temperature properties with good oxidation resistance. Different non-metallic additives such as AlN, ZrO_2, SiC, Si_3N_4, CrB_2, B_4C, TaC, TiC, WC, TiN, ZrN, ZrB_2 are reportedly used to obtain better with TiB_2 in combination with excellent high temperature mechanical properties [17-19, 33-34]. The microstructure of TiB_2-19.5 wt% ZrO_2-2.5/5.0 wt% SiC composite, processed via the hot isostatic pressing (HIP) route, reveals the presence of liquid phase (Ti, Zr)$_5$Si$_3$ formation at the triple point, which helps in the densification. Watanabe et. al [35] reported the formation of (Ti, Zr) B_2 solid solution in hot pressed TiB_2-30 wt. % ZrO_2 composites. Telle et. al [18] also reported the formation of (Zr,Ti,)O_2 solid solution in addition to (Ti,Zr)B_2 solid solution when 25 vol. % ZrO_2 is added to TiB_2. In another interesting investigation, Torizuka et al. [17] could not detect any noticeable solution formation, when 20 wt. % ZrO_2 binder was used to densify TiB_2 via HIP route.

According to Murata et al. [19] TaC and TaN were quite effective for densification of TiB_2. In their work, (Ti, Ta) B_2 and (Ta, Ti) (C, N) solid solutions were observed to form when TaC was added to TiB_2 and the composite was hot pressed at 2000^0C. SEM micrographs of the hot pressed TiB_2 specimens are shown in Fig. 2.3. The addition of binders influenced the sinterability and microstructure of the TiB_2 remarkably. Sintering additives enhances the density significantly and reduces the grain size by the secondary phase formation. Fig. 2.4 illustrates the fracture surfaces of TiB_2 specimens. The fracture of pure TiB_2 occurred mainly by an intergranular pattern (see Fig. 2.4a), apparently due to the high porosity and large grain size. TiB_2-based composites exhibited transgranular fracture. Reduction of pores, grain size and formation of secondary phases is also observed.
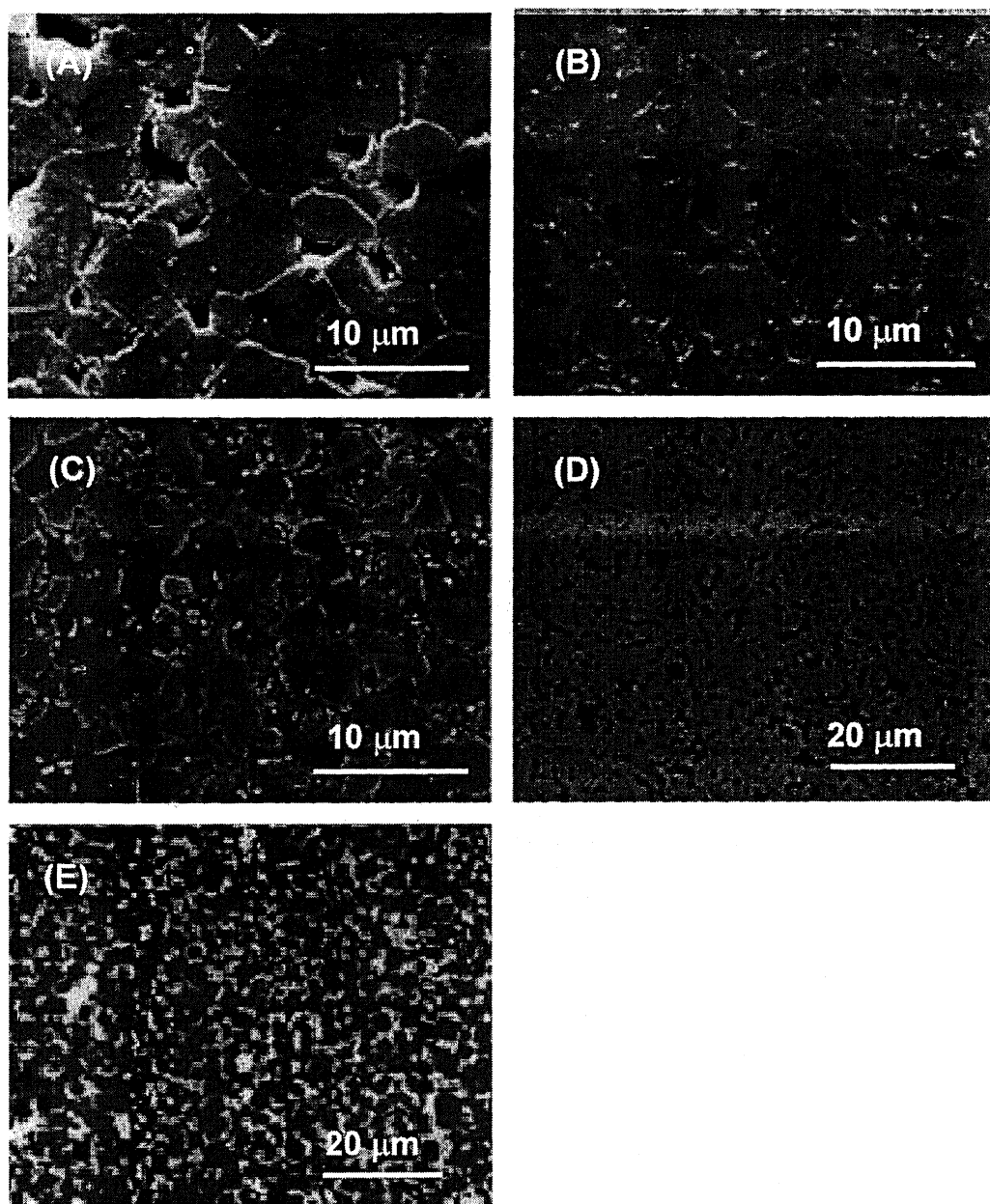
Fig. 2.3 Scanning electron micrographs of TiB$_2$ specimens hot-pressed at 1800^{0}C for 1h containing (A) 0 Wt%, (B) 2.5 Wt% Si$_3$N$_4$ and (C) 5 Wt% AlN, (D) 3.5 Wt% SiC and (E) TiB$_2$-based cermet with Ni$_3$(Al,Ti) binder [38,39].
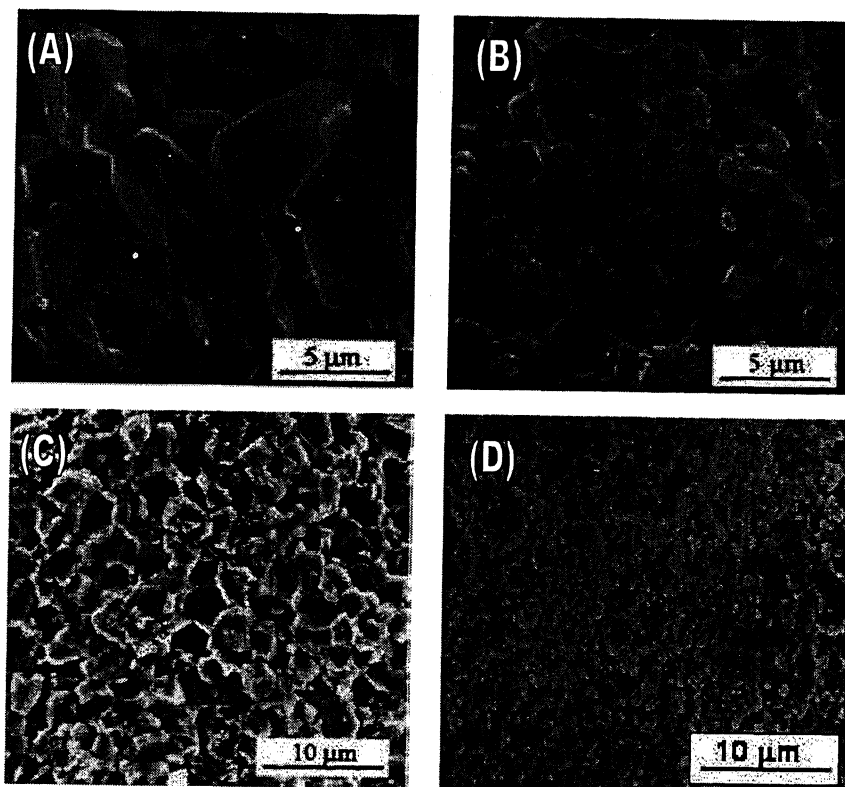
Fig. 2.4 Fracture surfaces of TiB₂ specimens containing (A) 0 Wt%, (B) 2.5 Wt% Si₃N₄, (C) 5 Wt% AlN and (D) 10 Wt% MoSi₂ [24,38,39].

Park et.al [37] reported the formation of different reaction products like TiN and BN in TiB_2–2.5-10 wt% Si_3N_4 composites, hot-pressed at 1800^{0}C. The relative density increased remarkably, to >99% ρ_{th}, when 2.5 wt% of Si_3N_4 was added. However, the density decreased slightly when more Si_3N_4 was added. The average grain size also was influenced strongly by Si_3N_4 addition. The hardness of the specimen also was improved by the addition of 2.5 wt% of Si_3N_4. The enhancement in density that resulted from the addition of Si_3N_4 was attributable to the improved mechanical properties. The addition of more Si_3N_4 caused the hardness to decrease, apparently because of the formation of secondary phases. Simillar trend also was observed for the flexural strength. In contrast to the strength or hardness, the fracture toughness decreased steadily as the amount of Si_3N_4 was increased. The high fracture toughness, obtained with pure TiB_2, is believed to be related to the large grain size and higher porosity.

In another work, Park et.al [38] investigated the effect of hot pressing temperature on the densification behavior of TiB_2. TiB_2 specimens were hot pressed for 1 hr at temperatures in the range of 1500-1800^{0}C, with an addition of 2.5 wt. % Si_3N_4 as a sintering aid. The sharp increase in density in temperature range (1500–1600°C) is believed to be related to the formation of silica (SiO_2) during hot pressing. Unlike the density, the average grain size increased steadily as the temperature increased. This result is in contrast to the case of transition-metal additions, where extensive grain growth occurs with densification. This microstructural evolution suggests that, to densify TiB_2 at low temperatures, the elimination of the oxide layer is necessary and the formation of a liquid phase during sintering is crucial.

The strength of TiB$_2$-2.5 wt. % Si$_3$N$_4$ composites increased sharply as the hot pressing temperature increased up to 1600°C, clearly because of the increase in density. However, at higher hot-pressing temperatures, the strength remained constant or decreased slightly. Similar trends were observed for the specimen hardness. However, the fracture toughness of the specimen that was hot-pressed at 1550°C was higher than that of any other specimens. Residual pores present in the specimen were indicated as one of the causes for this phenomenon. These results illustrate that TiB$_2$ with good mechanical properties can be densified at temperatures as low as 1600°C with the addition of 2.5 wt.% Si$_3$N$_4$ as a sintering aid.

Muraoka et.al. [34] reported the hot isostatic pressing of TiB$_2$- ZrO$_2$ composite. Dense sintered composites of TiB$_2$ and ZrO$_2$ (2 mol% Y$_2$O$_3$) have been fabricated by HIPing for 2h at 1500^{0}C under 196 MPa under argon atmosphere. The ZrO$_2$ particles in the composites are in monoclinic symmetry. No reaction product was identified. The fracture toughness and bending strength of the composites with 30-mol% ZrO$_2$ content were 11.2 MPa.m$^{1/2}$ and 680 MPa, respectively.

Li et.al. [39] investigated the densification and mechanical properties of titanium diboride (TiB$_2$), with aluminum nitride (AlN) as sintering aid. They recognized that the presence of AlN had a strong influence on the sinterability and mechanical properties of TiB$_2$, while hot pressed at 1800^{0}C due to the following mechanism. When a small amount of AlN ($\leq$ 5 wt. %) was added to the TiB$_2$, the rutile (TiO$_2$), present on the TiB$_2$ powder surface was eliminated by a reaction with AlN to form TiN and Al$_2$O$_3$.

The effect of SiC and ZrO$_2$ on sinterability and mechanical properties of titanium nitride, titanium carbonitride and titanium diboride was investigated by Torizuka et.al. [17]. The

combined addition of ZrO_2 and SiC were found to be effective in improving sinterability and mechanical properties of TiB_2. The density of TiB_2 and TiB_2-20 wt. % ZrO_2 after sintering at 1700^0C were 70 % of their theoretical densities. The addition of ZrO_2 had little effect in improving the sinterability of TiB_2. On the other hand, the density of TiB_2-19.5 wt. % ZrO_2-2.5 wt. % SiC was 97 % ρ_{th}. Although TiB_2 and TiB_2-20%ZrO_2 are lacking sinterability, the addition of SiC was very effective in improving the sintered density. The reason behind this is that TiO_2 existing on the surface of TiB_2 powder reacts with SiC and formed TiC and SiO_2.

Holcombe et.al. [40] reported the microwave sintering of titanium diboride. Using a 2.45 GHz, 6 KW microwave furnace adapted for inert gas sintering, titanium diboride (TiB_2) was rapidly microwave-sintered to >90% ρ_{th} of theoretical density at sintering temperatures of 1900 to 2100^0C and soak times of 30 min or less. Densification behavior with low-level additives was evaluated and the addition chromium diboride was found to be an effective sintering additive and grain growth inhibitor. A special covering system was used during the microwave sintering experiments to produce oxide free TiB_2. A comparison with conventional sintering indicated that microwave sintering of TiB_2–3wt% CrB_2 occurred at lower temperatures (i.e. 200^0C lower) and yielded material with significantly improved hardness, grain size, and fracture toughness.

Wen et.al [21] reported the reaction synthesis of TiB_2–TiC composites with enhanced toughness. In-situ toughened dense TiB_2-TiC_x composites were fabricated using reaction synthesis of B_4C and Ti powders at high temperatures. The reaction products mainly consisted of TiB_2 and TiC_x. No other phases, e.g. Ti_3B_4, TiB, Ti_2B_5 and free Ti, were observed. The microstructural morphology was characterized by TiB_2 plate-like grains

distributed uniformly in the TiC_x matrix. The characteristic microstructure exhibits high

fracture toughness (up to 12.2 MPa m$^{1/2}$). The very high reaction temperature (1800^0C)

was believed to be responsible for the formation of plate-like grains, which, in turn, was

responsible for the improved mechanical properties. The major toughening mechanisms

were likely to be crack deflection, platelet pullout and the micro-fracture of TiB_2 grains.

Tough TiB_2-TiC composites have also been successfully synthesized by means of in-situ

reaction of B_4C and Ti powder mixtures at relatively high temperatures [21]. The

synthesis of dense TiB_2–TiN nanocrystalline composites through mechanical and field

activation was investigated by Lee and Munir [41]. Powder mixtures of Ti, BN, and B

were mechanically activated via ball milling. Vickers microhardness measurements

(at 2N) on the dense samples provided hardness values ranging from 14.8 to 21.8 GPa

and fracture toughness (at 20 N) values ranging from 3.32 to 6.50 MPa m$^{1/2}$, depending

on the processing conditions.

Synthesis of $MoSi_2$–titanium boride composites via in situ displacement reactions was

reported by Silva et. al [42]. The $MoSi_2$-TiB₂ composites, produced by in-situ

displacement reactions possessed very fine microstructures that could not be achieved

when the staring materials were elemental powders, i.e. when no displacement reaction is

involved. No evidence of liquid phase formation could be found in any of the samples,

while the formation of intermediate silicides seems to be an important part of the process.

When the elemental powder reacts, no intermediate boride phases could be identified.

Naka et.al. [43] fabricated TiB_2 compacts by hot pressing the synthesized TiB_2 powder,

which was obtained by a solid-state reaction between TiN and amorphous boron.

Densification of the compacts occurred at 1800^0C under 20 MPa pressure for 5 to 60 min

with the aid of a reaction sintering. A homogeneous sintered (98% ρ_{th}) single phase TiB_2, prepared by hot pressing for 30 min from the starting powder composition [(TiB_2 + 0.2 B) + 0.1 Ti], exhibited a fine-grained microstructure composed of TiB_2 grains with diameters of 2 to 3μm. The microhardness, transverse rupture strength and fracture toughness of the TiB_2 sintered compact were reported to be 28.5 GPa, 480 MPa and 2.4 $MPa.m^{1/2}$ respectively.

2.5 Outlook

Transition borides, an important class of advanced structural ceramic materials, are potential materials for versatile application i.e. armor materials, aluminum evaporation boat, cathode material for hall-heroult cell, cutting tool, EDM electrode, wear resistance applications, high temperature applications, electrical assisted devices, in aerospace applications, in foundry/refractory applications and various other miscellaneous applications. Despite the excellent properties, the engineering applications of monolithic TiB_2-based ceramics as high temperature structural materials is limited due to poor sinterability, brittleness and low oxidation resistance. Various metallic and nonmetallic binders have been used to obtain dense borides. The metallic additive allows densification to occur effectively via liquid phase sintering. However, the presence of metallic binder is not desirable for high temperature structural applications. Therefore studies have also been carried out with non-metallic additives to improve sinterability and also to retain mechanical properties at high temperature with good oxidation resistance. The non-metallic additives react with surface oxide layers and leads to formation reaction products which in turn results in better densification and properties. In future, the

advanced sintering techniques like Spark Plasma Sintering (SPS) could be adapted to achieve faster densification and better properties. Also, new sinter-additives can be used and the processing as well as material parameters should be optimized to obtain better mechanical properties in a designed microstructure.

2.6. Reference:

[1] V. J. Tennery, C. B. Finch, C. S. Yust and G. W. Clark, Ed: Viswanadhan et.al. , "Structure-property correlations for TiB$_2$-based ceramics Densified using active liquid metals", Science of Hard Materials, 891-909, Plenum, New York, (1983).

[2] B. Todd, "Energy Reduction in Hall-Heroult Cells with conventional and special electrodes", J. Met., 33 [9] 42-45 (1981).

[3] J. M. L. Wilkins, " Boron and Refractory borides", edited by V. I. Matkovich (Spring-verlag, New York, 633 (1977).

[4] Mroz. C., Titanium diboride, Am. Ceram. Soc. Bull., , 74 158-159 (1995).

[5] Matkovich, V. I., Boron and Refracotry Borides, Spring, Berlin, 172 (1997).

[6] M. Einarsrud, E. Hagen, G. Petterson and T. Grande, "Pressureless Sintering of Titanium diboride with Nickel, Nickel boribe and iron additives", J. Am. Ceram. Soc., 80 [12] 3013-3020 (1997).

[7] M. K. Feber, P. F. Becher and C. B. Finch, "Effect of microstructure on the properties of the TiB$_2$ ceramics", J. Am. Ceram. Soc., 66 [1] C2-C4 (1983)

[8] C. B. Finch, P. F. Becher, P. Angelini, S. Baik, C. E. Banberger and J. Brynestod, "Effect of impurities on the densification of submicormeter TiB$_2$ powders", Adv. Ceram. Mater, 1 [1] 50-54 (1986).

[9] G. Petzow, R. Telle, New Development in the field of refractory hard metals based on cemented borides in: S. Somiya (Ed.), Advanced Ceramics, Terro Scientific Publishing Company, Tokyo, 131-143 (1987).

[10] Z. T. Zakhariev, M. S. Ivanova, I. Serebriankova, Hard materials based on cemented TiB2-WC-Co alloys, Z. Metalkal. 85 [11] 801-803 (1994).

[11] T. Graziani and A. Bellosi, "Sintering and characterization of TiB$_2$-B$_4$C-ZrO$_2$ composites", Materials and Manufacturing Processes, 9 [4] 767-780 (1994).

[12] S. H. Kang, D. J. Kim, E. S. Kang and S. S. Baek, Pressureless Sintering and Properties of Titanium Diboride Ceramics Containing Chromium and Iron, J. Am. Ceram. Soc., 84 [4] 893-895 (2001).

[13] D. G. Ahn, A. Kawasaki, R. Watanabe, Microstructure and Mechanical properties of TiB_2 −W cermets prepared by HIP, Mater. Trans. JIM 37 [5] 1078-1083 (1996).

[14] S. Torizuka, K. Sato, J. Harada, H. Yamamot and H. Nishio, "Microstructure and sintering mechanism of TiB_2-ZrO_2-SiC composite", J. Ceram. Soc. Japan, 100 [4] 392-397 (1992).

[15] S. Torizuka, K. Sato, H. Nishio and T. Kishi, "Effect of SiC on interfacial reaction and sintering mechanism of TiB_2", J. Am. Ceram. Soc., 78 [6] 1606-1610 (1995).

[16] J. Ho Park, Y. Koh, H. Kim C. Hwang and E. Kong, "Densification and Mechanical Properties of Titanium Diboride with Silicon Nitride as Sintering Aid", J. Am. Ceram. *Soc.,* 82 [11] 3037-3042 (1999).

[17] S.Torizuka and T.Kishi, "Effect of SiC and ZrO_2 on sinterability and mechanical properties of titanium nitride, titanium carbonitride and titanium diboride," Materials Transactions, JIM, 37 [4] 782-787 (1996).

[18] R. Telle, S. Meyer, G. Petzow and E.D. Franz, "Sintering Behavior and Phase Reactions of TiB_2 with ZrO_2 Additives," Materials Science and Engineering *A* 105/106 125-129 (1988).

[19] Y. Murata, H.P. Julien and E.D. Whitney, "Densification and wear resistance of ceramic systems: I. Titanium Diboride," *Ceramic Bulletin,* 46 [7] (1967).

[20] H-Jong Kim, H-J Choi and J-G Lee, Mechanochemical Synthesis and Pressureless Sintering of TiB_2-AlN Composite, J. Am. Ceram., 85 [4] 1022-1024 (2002).

[21] G. Wen, S. B. Li, B.S Zhang and Z. X. Guo, Reaction Synthesis of TiB_2-TiC Composites with enhanced toughness. Acta mater. 49 1463-1470 (2001).

[22] A. K. Vasudevan, J. J. Petrovic, A comparative Overview of molybdenum disilicde composites, Mater. Sci. Eng. A 155 1-2 (1992).

[23] A. Costa e Silva and M .J. Kaufman, Mater. Sci. Eng. A 195 [1] 75-88 (1998).

[24] T. S. R. Ch. Murthy, B. Basu, R. Balasubramaniam, A. K. Suri, C. Subramanian and R. K. Fotedar, Processing and properties of Novel TiB_2-based composites, communicated to J. Am. Ceram, August 2004.

[25] B. Basu, J. H. Lee and D. Y. Kim, "Development of Nanocrystalline wear resistant Y-TZP ceramics", J. Am. Cer. Soc., 87 [9] 1771-1774 (2004).

[26] S. W. Wang, L. D. Chen and T. Hirai; Densification of Al$_2$O$_3$ powder using spark plasma sintering; J. Mat. Res., 15[4] 982 (2000).

[27] J. R. Groza, A. Zavalianges, Sintering Activation by external electric field, Mat. Sci. and Engg., A287 171-177 (2000).

[28] G.V.D. Goor, P. Sägesser and K. Berroth, *"Solid State Ionics,"* 1163 101-103 (1997).

[29] M. Berger, M. Larsson and S. Hogmark, "Evaluation of magnetron-sputtered TiB$_2$ intended for tribological applications," *Surface and coatings Technology*, 124 253-261 (2000).

[30] Ronald G. Munro, "Material properties of titanium diboride," *J. Res. Natl. Inst. Stand. Technol.*, 105 [5] 709-720 (2000).

[31] M.V. Swain, "structure and properties of ceramics", in: *Materials Science and NY(USA),*V.11 (1993)175-258.Technology, ed. R.W.Cahin, P.Haasen, and E.J.Kramer, VCH publishers Inc.

[32] S. Baik and P.F. Becher, "Effect of oxygen contamination on densification of TiB$_2$," J.Am.Ceram.Soc, 70 [8] 527-30 (1987)

[33] D.E.Mahagin and R.E.Dahl, "Nuclear applications of boron and the borides", in: *Boron and refractory borides, ed.* V.I.Matkovich, Springer- Verlag Berlin Heidelberg 613-632 (1977).

[34] Y. Muraoka, M. Yoshinaka, K. Hirota and O. Yamaguchi. "Hot Isostatic Pressing of TiB$_2$-ZrO$_2$ (2 Mol% Y$_2$O$_3$) composite powders," *Materials Research Bulletin,* 31 [7] 787-792 (1996).

[35] T. Watanbe and K. Shoubu, "Mechanical Properties of Hot–Pressed TiB$_2$-ZrO$_2$ Composites," *J.Am.Ceram.Soc.*, 68[2] C34-C36 (1985).

[36] E.S. kang and C.H. Kim, "Improvements in mechanical properties of TiB$_2$ by the dispersion of B$_4$C particles," *Journal of Materials Science*, 580-584 (1989).

[37] J.H. park, Y.H. Koh, H.E. Kim, C.S. Hwang and E. Kong, "Densification and Mechanical Properties of Titanium Diboride with Silicon Nitride as a Sintering Aid," *J.Am.Ceram.Soc.* 82 [11] 3037-3042 (1999).

[38] J.H. park, Y.H. Lee, Y.H. Koh, H.E. Kim and S.S. Baek, "Effect of Hot-Pressing Temperature on Densification and Mechanical Properties of Titanium Diboride with Silicon Nitride as a Sintering Aid," *J.Am.Ceram.Soc.* 83 [6] 1542-1544 (2000).

[39] L. H. Li, H.E. Kim and E.S. Kang, "Sintering and mechanical properties of titanium diboride with aluminum nitride as a sintering aid," *Journal of the European Ceramic Society,* 22 973-77 (2002).
[40] C.E. Holcombe and N.L. Dykes, "Microwave Sintering of titanium diboride," *Journal of Materials Science* 26 (1991), 3730-3738.

[41] J.W. Lee and Z. A. Munir, "Synthesis of Dense TiB_2 – TiN Nanocrystalline Composites through Mechanical and Field Activation," *J. Am. Ceram. Soc,* 84 [6] 1209-16 (2001).

[42] A.C. de Silva & M.J. Kaufman, "Synthesis of $MoSi_2$ – boride composites through in situ displacement reactions," *Intermetallics* 5 1-15 (1997).

[43] S. Naka and H. Hamamoto, "Preparation of TiB_2 sintered compacts by hot pressing," *Journal of Materials Science,* 25 533-536 (1990).

Chapter 3

Experimental

3. Experimental

3.1 Starting powders and densification

3.1.1 TiB_2/$MoSi_2$ composite

The in-house synthesized TiB_2 and $MoSi_2$ were selected as starting powders. TiB_2 is produced by borothermic reaction among TiO_2 (> 99% purity, Merck, Germany), B_4C (In-house) and C. This yielded TiB_2 with oxygen and carbon as major impurities. $MoSi_2$ powders are processed from elemental Mo (> 99% purity, supplier Leco Industries, U.S.A) and Si (>99% purity, supplier Merch, Germany). The details of the starting powders are given in Table. 3.1. The mean particle diameter and particle size distribution was measured using laser particle analyzer (Analysett 22). The specific surface area was measured by BET (COULTER, SA300). Planetary milling of TiB_2 and $MoSi_2$ starting powders in weight ratio of 90:10 was conducted with WC milling balls for 24 hours using acetone as a milling media to obtain mixed powders and to break the agglomerate.

Appropriate weight of premixed powders was placed in a graphite mold of 10 mm internal diameter with proper graphite insulation around it to prevent interaction of powders with graphite mold. The graphite punches are inserted into the mold and the graphite mold is placed in between the graphite electrodes of SPS chamber, which transfers load and current during SPS experiments. The SPS chamber is closed firmly and high vacuum of 70 mtorr is maintained throughout the experiment. DC current of 1- 1.5 kA and DC voltage of 5-10 V are applied and variation in this range depends on the final holding temperature. The experiments are carried out in the temperature range of 1300 – 1500°C with a heating rate of 600 K/min with holding time of 10 m. The pressure is slowly increased as the heating continues and a maximum pressure of 40 MPa is applied

at the holding temperature. The current flow is stopped and pressure is released as soon as the holding at sintering temperature is over. Fig. 3.1 revealing the various units associated with Spark Plasma Sintering machine.

Table. 3.1. Details of the starting powders used in the present investigation.

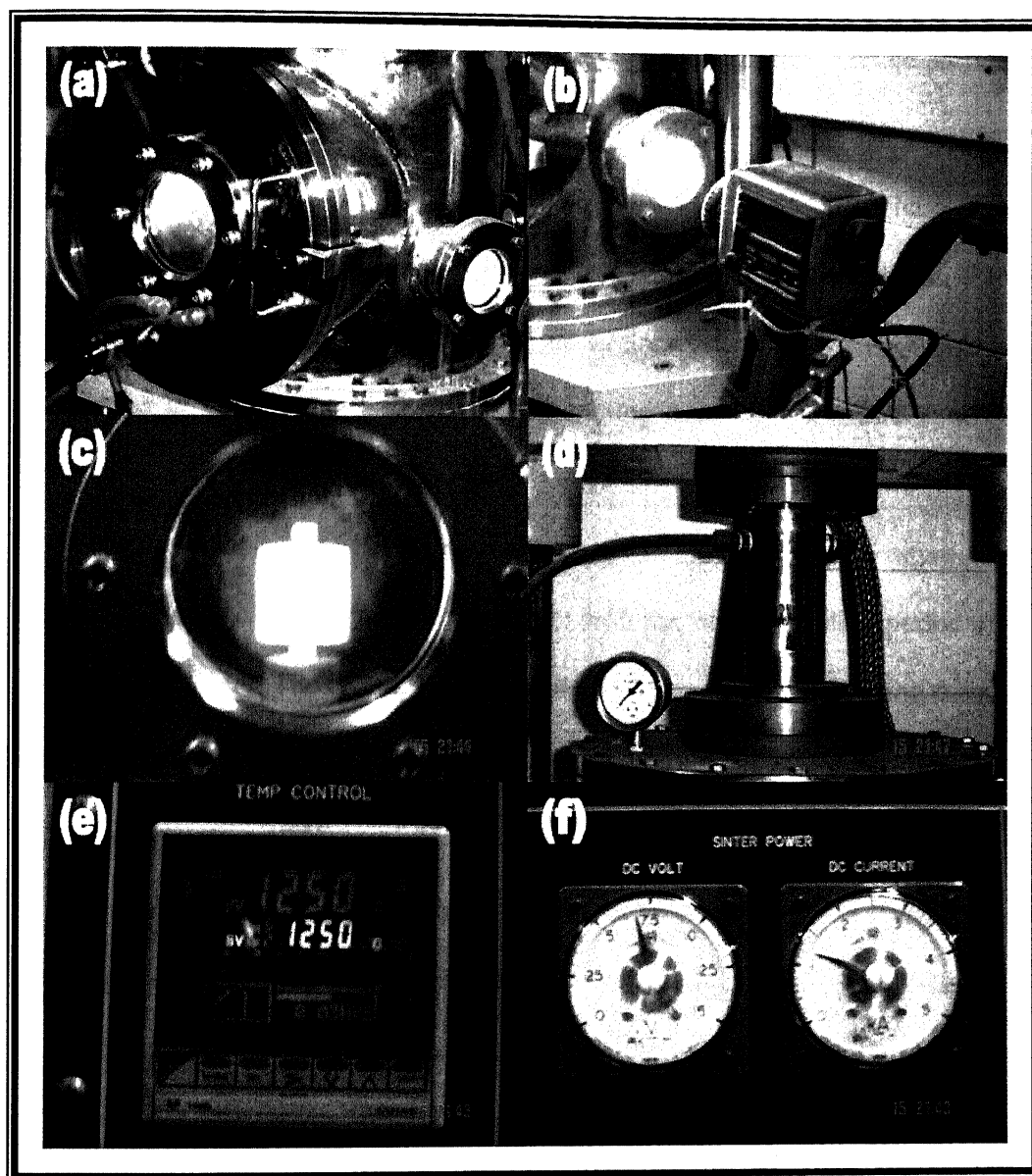| Powder	Supplier	Carbon (wt. %)	Oxygen (wt. %)	Nitrogen (wt. %)	Metallic Impurities (wt. %)	Median particle diameter, D_{50} (μm)	Surface area (m^2/g)
TiB_2	In-house	0.6	0.5	0.6	-	1.1	1.360
$MoSi_2$	In-house	0.37	0.3	-	-	1.4	0.389
TiO_2	Merck, Germany	-	-	-	Pb$\leq$0.005 As$\leq$0.0005 Fe$\leq$0.005	0.8	-
B_4C	In-house	19.5	-	-	Fe $\sim$ 2000ppm Si $\sim$ 2000ppm	6.7	-

Fig. 3.1 Spark Plasma sintering unit at Prof. DY Kim's Laboratory, SNU, S. Korea, exhibiting various units associate with SPS are heating chamber (a), optical pyrometer unit to measure temperature (b), Red hot graphite containing sintered material (c), ram to transfer load and current (d), Temperature monitoring controller (e) and DC current and voltage controllers (f).

3.1.2 TiB$_2$/Cu cermet

For the processing of TiB$_2$/Cu cermets, commercial available TiB$_2$ (average particle size

< 5 μm, Aldrich, USA) was used as the major phase in our composite. The commercially

available high purity copper (<5 μm, Aldrich, Korea) is used as a second phase. TiB$_2$: Cu

in the weight ratio of 94:6 was mixed in a planetary ball mill for 24 hours in 1 litre of

touelene in a polyethylene bottle. To break the agglomerates and to ensure appropriate

dispersion, WC balls were used during the mixing process. The powder mixing is

followed by drying in the oven.

To densify the cermets, the SPS experiments are carried out in the temperature range of

1200– 1500°C with a heating rate of 500 K/min with the varying holding period of 10 m

and 15 m respectively. The constant pressure of 40 MPa is maintained during the heating

and holding period. Other details of the SPS experiments are already mentioned above.

3.2 Characterization

After complete removal of graphite sheet layer around the specimen, the density of spark

plasma synthesized samples was measured in water following Archimedes principle. The

theoretical densities of composite were calculated by rule of mixture, taking 4.52 gm/cc,

6.24 gm/cc and 8.9 gm/cc for TiB$_2$, MoSi$_2$ and Cu respectively. Further, phase

identification was performed using X-ray diffraction using Cu Kα radiation (Rich-Seifert,

2000 D). The Elastic Modulus (E) was measured using pulse-echo resonance frequency

method (Tektronix TDS 200, Panametrics Model 5800). The Vickers Indentation is

carried out on well polished surface to measure hardness and toughness at load of 10 kg

with a dwelling time of 15 sec on a Universal Hardness tester. The Fracture toughness is

evaluated by crack length measurement (2a) around the radial crack pattern formed by

Vickers indentation adopting formulation proposed by Anstis et al. (Fig. 3.2) [1]. The reported values are the average of five indentation tests. Detailed Microstructural investigation of the polished and fractured composites was performed using Scanning Electron Microscopy (FE-SEM, JSM-6330F) Elemental analysis of different phases are examined using EDS equipped with SEM. Electrical resistivity (dc) of all the SPS processed samples was measured by standard four probe method at room temperature with appropriate silver epoxy-coating on the flat materials, followed by hardening at 150°C.

Vickers, load P

$$K_{IC} = \zeta(E/H)^{1/2}(P/c^{3/2}) = T_0$$

$$(\zeta = 0.016)$$
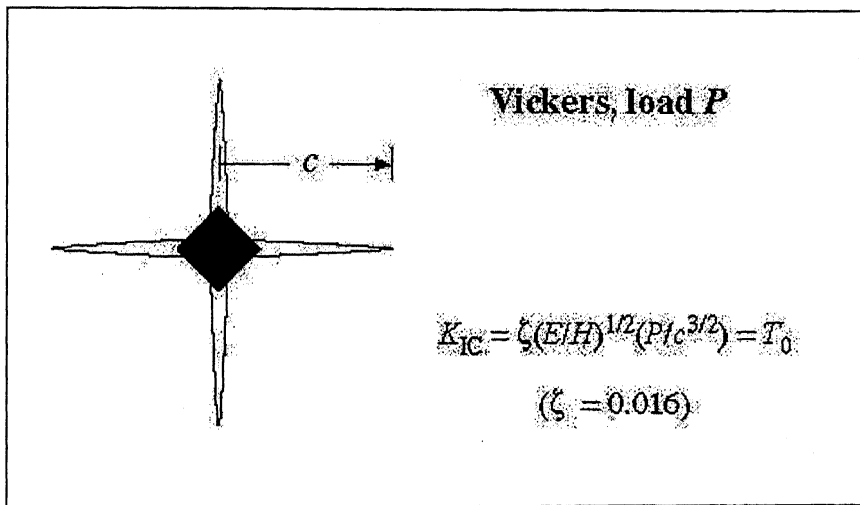
Fig. 3.2. Schematic of the indentation toughness measurement, as followed in the present work, usually performed for brittle materials like ceramics. The toughness is calculated from the measured lengths of surface radial cracks emanating from the indentation corners [1].

3.3 Reference

[1] Anstis, G. R., Chantukul, P. Lawn, B.R. and Marshall, D.B., "A critical evalution of indentation techniques for measuring fracture toughness", J. Am. Cer. Soc., 64, 553-557 (1981).

Chapter 4

Results and Discussion
*   -TiB$_2$/MoSi$_2$ Composite*

4. Results and Discussion

4.1 Densification

The densification data of the developed TiB_2-based composites and corresponding monolithic (TiB_2 and $MoSi_2$) materials are presented in Fig. 4.1 and Table 4.1. Monolithic TiB_2 and $MoSi_2$ exhibit maximum densification of ~98 %ρ_{th} and ~95 %ρ_{th} respectively at the SPS temperature of 1400°C under identical sintering conditions. Also, monolithic boride and silicide materials exhibit a slight decrease in sintered density with increase in SPS temperature from 1400 to 1500°C. For the composite, the density increase with SPS temperature and exhibits maximum densification (~ 98 % ρ_{th}) at the SPS processing temperature of 1400°C for a holding period of 10 min. A similar trend in densification is observed with further increase in sintering temperature to 1500°C.

In general, conventional pressureless sintering of the TiB_2 based materials are carried out in the temperature range greater than 1800°C and the densification is generally assisted i.e. enhanced with application of pressure (HIP, HP) [1,2]. SPS route therefore enables attractive in the densification of borides at temperature of 400-500°C lower than other conventional sintering technique. This temperature difference in the case of borides is significant when compared with oxide ceramics. Moreover temperature difference form centre to core of the specimen placed inside the graphite die will be much more in conductive ceramics like TiB_2 and temperature profile in SPS regarding for various materials is not elucidated [3]. In reviewing the mechanism of plasma sintering, initial voltage supplied combined with mechanical pressure result in the breakdown of oxide layer present over the surface of the constituent ceramic powder particles, followed by arching and evaporation of the surface product due to plasma formation [4]. Moreover, the prolonged sintering time of 15 min of monolithic TiB_2, yielding densification more

Table. 4.1. Mechanical and electrical properties of the TiB$_2$, TiB$_2$ - 10 wt. % MoSi$_2$ composite and MoSi$_2$ materials, Spark Plasma Sintered at different temperature range for a holding period of 10 min under a pressure of 40 MPa in vacuum.

| Sample Composition	SPS Temperature (°C)	Density (gm/cc)	ρ_{th} (%)	Elastic Modulus (E, GPa)	Vickers Hardness (Hv_{10}, GPa)	Fracture Toughness (K_{Ic}, MPa m$^{1/2}$)	Electrical Resistivity (ρ, $\mu\Omega$-cm)	Electrical Conductivity ($1/\rho$, MΩ^{-1}-cm^{-1})
TiB$_2$ - 10 wt.% MoSi$_2$	1300	4.42	94.22	318.4	13.9 ± 0.6	3.6 ± 0.5	10.92	0.092
TiB$_2$ - 10 wt.% MoSi$_2$	1400	4.58	97.54	393.6	16.0 ± 0.2	3.8 ± 0.3	11.99	0.083
TiB$_2$ - 10 wt.% MoSi$_2$	1500	4.57	97.47	391.2	16.3 ± 0.2	4.5 ± 0.1	12.38	0.081
TiB$_2$	1400	4.41	97.64	428.1	17.3 ± 0.6	4.8 ± 0.8	13.26	0.075
TiB$_2$	1500	4.34	96.12	397.9	16.4 ± 0.3	4.4 ± 0.4	–	–
MoSi$_2$	1400	5.94	95.26	330.8	9.9 ± 0.1	2.9 ± 0.1	18.87	0.053
MoSi$_2$	1500	5.91	94.73	332.2	9.5 ± 0.2	2.8 ± 0.3	16.62	0.060
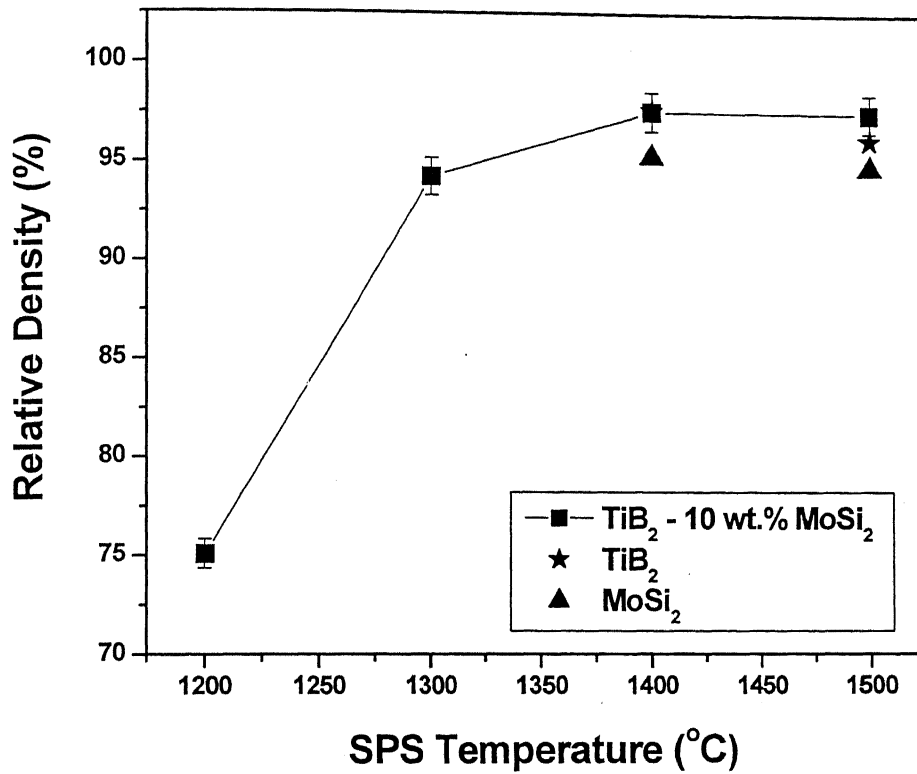
Fig. 4.1. Plot of relative density versus spark plasma sintering temperature for monolithic TiB₂, TiB₂- 10 wt. % MoSi₂ composite and monolithic MoSi₂.

than 99 % indicates attaining full densification in SPS route for difficult to sinter materials like borides is possible. From these results, we believe that grain boundary cleaning and binderless sintering of TiB_2 is feasible through the SPS processing route. It can be noted that Torizuka et. al achieved 95% ρ_{th} with TiB_2–2.5 wt % SiC composite, when hot pressed at 1700^0C [1]. Also 98% ρ_{th} was obtained with TiB_2-5 wt % AlN, hot pressed at 1800^0C by Li et. al [5]. Park et. al achieved 99% ρ_{th} using 2.5 wt % Si_3N_4 additives for TiB_2 hot pressed at 1800^0C for 1h [6]. Also, our recent work revealed that monolithic TiB_2 can be hot pressed to ~98%ρ_{th} at 1800°C, similar density in TiB_2- 10 wt.% $MoSi_2$ composite could be achieved after hot pressing at 1800°C under identical conditions (1h, vacuum). From the above it clear that the addition of 10 wt. % $MoSi_2$ and plasma assisted sintering provides better densification of the composite material at much lower temperature and sintering time compared to the hot processing condition (1700°C, 1hr).

4.2. Microstructure

The microstructural characterization of the SPSed materials are also carried out in order to understand the densification mechanism and to establish microstructure-property relationship. Fig. 4.2 presents XRD analysis of the TiB_2-10 wt. % $MoSi_2$ composite, SPSed at 1400^0C and 1500^0C, revealing the presence of the various crystalline phases. Besides the predominant presence of TiB_2 and $MoSi_2$, the noticeable presence of $TiSi_2$ could be easily detected in the composite. The presence of SiO_2 or B_2O_3 was not detected within the resolution limit of XRD. The obtained XRD data however indicate the occurrence of sintering reaction leading to the formation of $TiSi_2$, which will be discussed later.
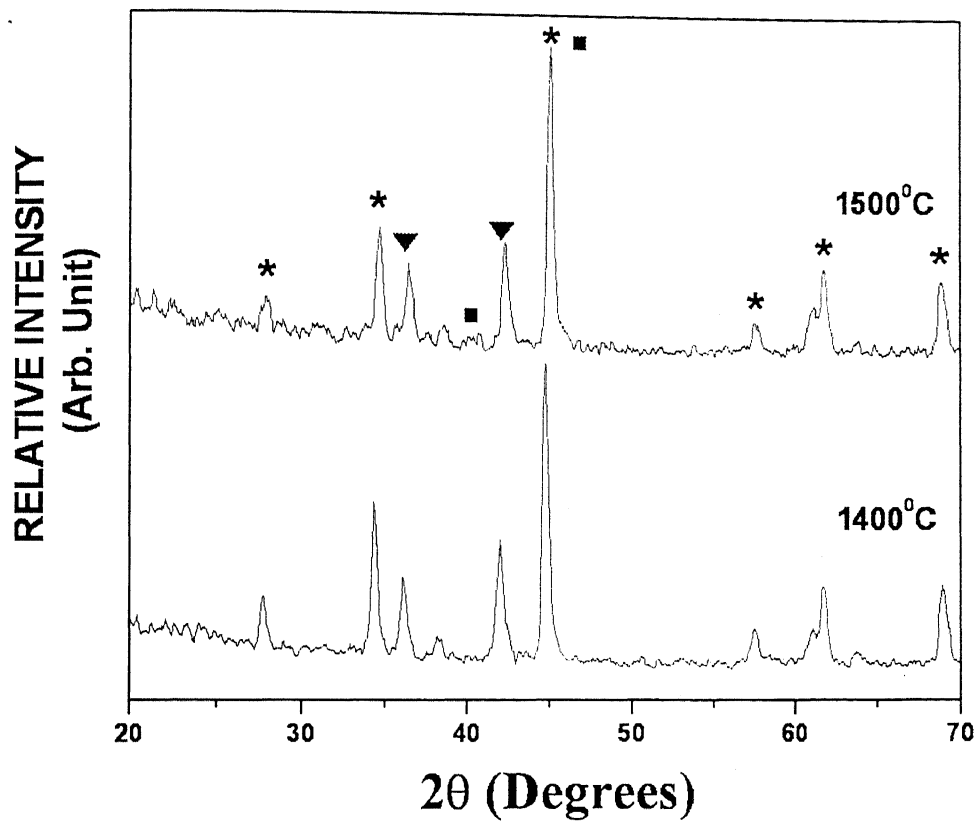
Fig. 4.2. X-ray diffraction pattern of TiB$_2$- 10 wt. % MoSi$_2$, SPSed at 1400°C and 1500°C for 10 min under vacuum (c). The different crystalline phases are TiB$_2$ (*), MoSi$_2$ (■), TiSi$_2$ (▼).

Fig.4.3 shows the SEM images of the starting powders, revealing the particle sizes of TiB_2 and $MoSi_2$ as 0.5-2 µm and 2-3 µm respectively. Also TiB_2 particles are of spherical shape, whereas $MoSi_2$ particles are of sharply faceted and of irregular shape.

SEM images of the fracture surfaces of the monolithic TiB_2 and $MoSi_2$ are depicted in the Fig. 4.4 Monolithic TiB_2, with maximum densification (~ 98 % ρ_{th}), after SPSed at 1400^0C for 10 min, is characterized by the presence of the isolated pores. Also, the fracture surface of the monolithic TiB_2 shows the presence of well faceted equiaxed TiB_2 grains with intercrystalline pores trapped between the grains and at the triplet junction (Fig. 4.4a). The microstructure of monolithic TiB_2 material is characterized by the average grain size of 2-5 µm. The observed fracture mode in the monolithic TiB_2 is purely intergranular in nature. Fig. 4.4b presents the fracture surface topography of SPSed monolithic $MoSi_2$. The fractograph is characterized by disintegration of $MoSi_2$ particles (grey contrast) leading to loss of particle shape. In fact, it is difficult to characterize the microstructure with a specific grain size. In a SPS study, significant grain growth was observed for $MoSi_2$ with grain sizes increasing from 5 to 30 µm as SPS temperature increased from 1200 to 1500°C with holding of 10 minutes at each temperature. Moreover the observed growth is more in comparison with other oxide ceramics [3]. Additionally, EDS analysis of SPSed $MoSi_2$ (our sample) reveals that the black contrast phase is SiO_2. Observing Fig. 4.4b closely reveals that SiO_2 phase probably has melted during SPS processing. Some SiO_2 particles are also observed to be present in the intercrystalline region. The topographical features implicate that the dominant fracture mode is transgranular in nature. The formation of SiO_2 can be linked to
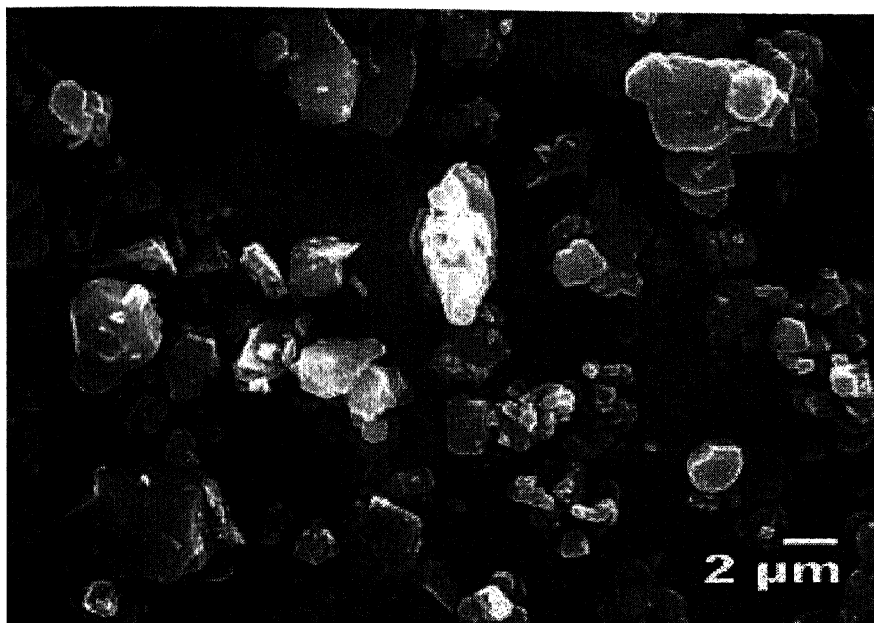
(a)
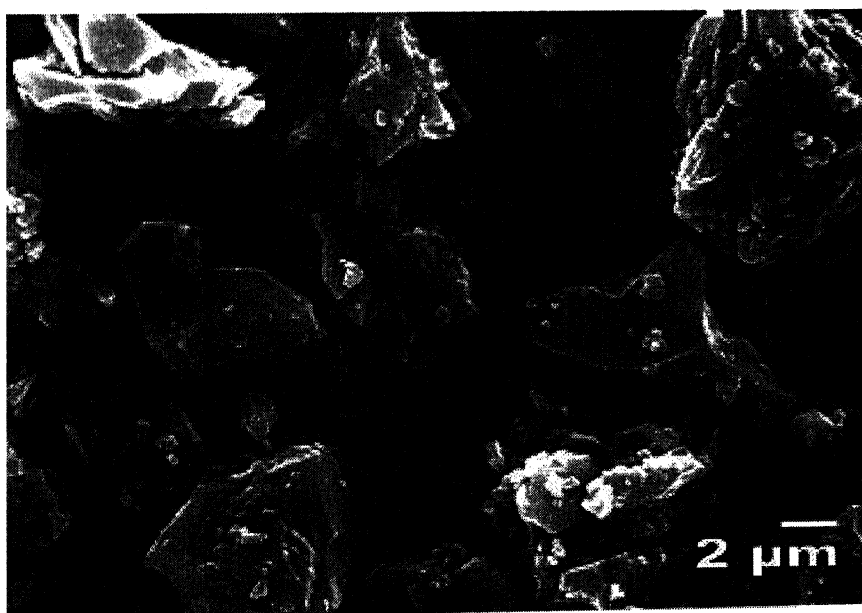
(b)

Fig. 4.3. SEM images showing the morphology of TiB₂ (a) and MoSi₂ (b) starting powders.

(a)

(b)

Fig. 4.4. Scanning electron micrographs of fracture surfaces of monolithic TiB₂ Spark Plasma Sintered at 1400°C for 10 min, showing the presence of intercrystalline pores between grains and triplet junction (a) and monolithic MoSi₂, SPS processed at 1400°C for 10 min reveals the presence of SiO₂ inclusion (black) at the grain boundaries and triplet junction (b).
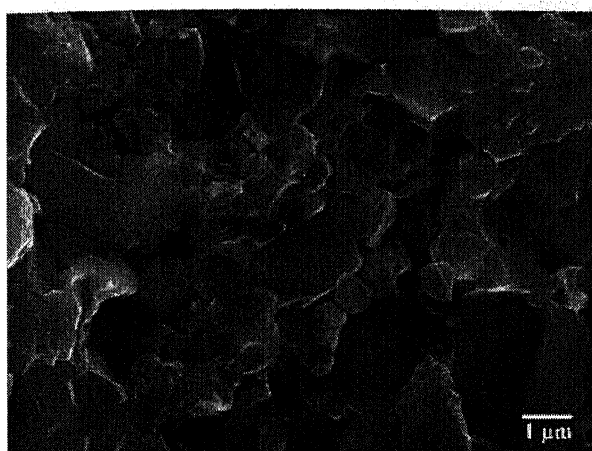
(a)
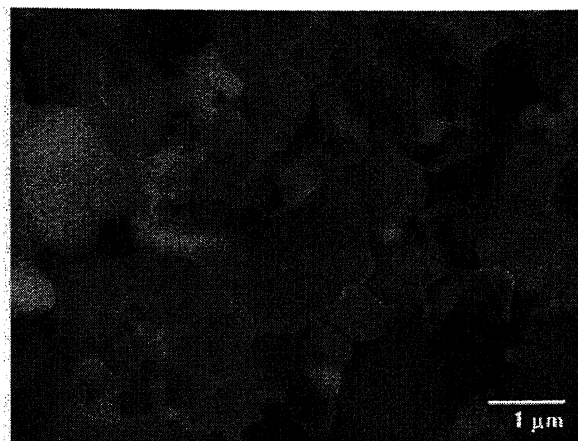
(b)
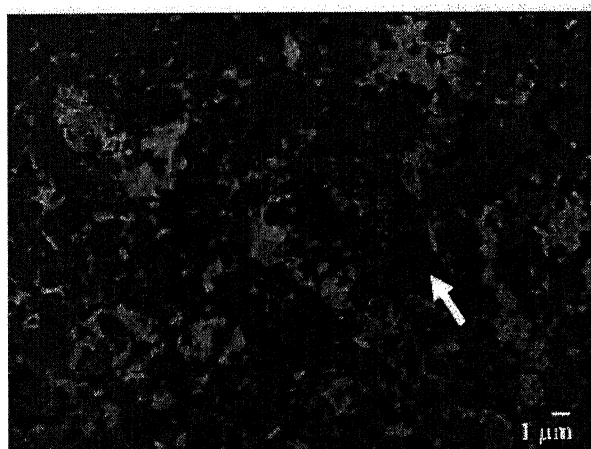
(c)
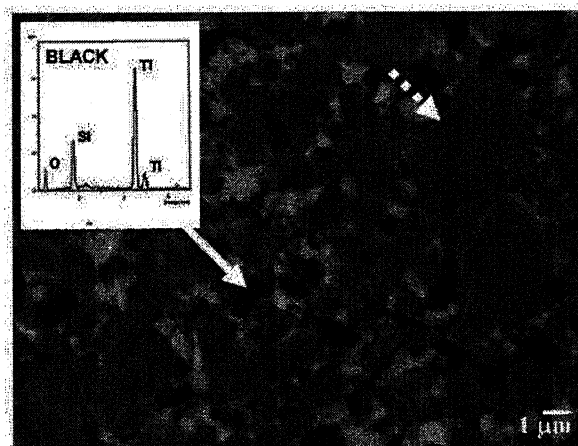
(d)

Fig. 4.5. Fractography of TiB₂-10 wt. % MoSi₂ composite SPS processed at 1400°C for 10 min showing mixed intergranular and transgranular fracture mode (a) and BSE mode of fracture surface of same composite (b), revealing white contrast phase as MoSi₂ (b). SEM images of polished surface revealing three phases: TiB₂ (grey), MoSi₂ (bright) and TiSi₂ (dark) respectively (c & d).The abnormal growth of few TiB₂ grains are also indicated by dotted arrow (d). EDS result of the black phase (reaction product, TiSi₂) can also found as an insert in (d).

the 'Pest behavior' of $MoSi_2$, which can be explained by a thermodynamically feasible reaction (favorable upto 3327°C) [7-9]:

$$MoSi_2 (s) + 7/2 \, O_2 (g) \quad \rightarrow \quad MoO_3 (g) + 2SiO_2(l)$$
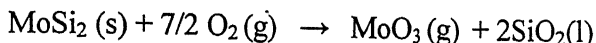
Due to high vapor pressure at low temperature, MoO_3 is volatilized and results in the retention of SiO_2 in the sintered microstructure. In the SPS sintering, generation of Spark plasma results in the vaporization and melting of SiO_2 protective layer on the particle surface. This, in combination with TiO_2 layer of TiB_2 chemically could possibly react to form $TiSi_2$ reaction product. This can be a potential reaction mechanism, however this will be discussed in details in section 4.4.

Fig.4.5 presents the SEM images of the fracture and polished surfaces of the developed TiB_2- 10 wt. % $MoSi_2$ composite material, optimally SPSed at 1400°C for 10 minutes. The developed composite exhibits the mixed mode of intergranular and transgranular fracture (Fig. 4.5a & b). Figs. 4.5c & d illustrate the backscattered electrons micrographs obtained from the polished surfaces. The wider atomic number difference among the constituent phases enables in distinguishing various phases. The microstructure is characterized by the three phases with grey, black and white contrast. EDS analysis of different phases confirms that the grey and white phases are TiB_2 and $MoSi_2$ respectively. While the third phase with black/dark contrast is rich with Ti and Si (see insert of Fig. 4.5d). This observation along with XRD results confirms that the black phase probably is $TiSi_2$. An interesting observation that the average grain size of $MoSi_2$ is ~3-5 μm and moreover the disintegration of that phase has occurred. It is clear from the microstructure that $TiSi_2$ reaction product, being liquid at ~1500°C helps in the densification and well bonding of the TiB_2 based composite material. The average grain size of the TiB_2

particles in the composite is in the range of 1-3 μm. Occasionally, coarser TiB_2 particles in the composite of sizes more than 5 μm also are observed (Fig. 4.5d). The grain growth in the SPSed TiB_2 samples can be ascribed to high conductivity of TiB_2 and the electric current effect, inherent in SPS processing. Moreover the grain growth of the TiB_2 grain in the composite material is lower in comparison with the monolithic TiB_2. This fact supports the suppression of the grain growth of TiB_2 due to grain boundary pinning by $MoSi_2$.

4.3. Mechanical and Electrical property

Fig.4.6 plots the hardness and fracture toughness of the developed materials as a function of SPS temperature. The developed TiB_2-10 wt. % $MoSi_2$ composite exhibits maximum hardness of ~16.5 GPa when sintered at 1400°C and an increase in trend of hardness is measured with increase in SPS temperature from 1300°C to 1400°C. No significant change in mechanical property of the composite for varying SPS temperature of 1400°C and 1500°C is observed. The Elastic-modulus of the developed composite material is ~390 GPa, which is lower than that of monolithic TiB_2. The fracture toughness of the composite varies from 3.9 to 4.5 MPa $m^{1/2}$ and exhibits higher value when SPSed 1500°C. The monolithic TiB_2, SPSed at 1400°C exhibits hardness of 17.5 GPa and fracture toughness of 4.8 MPa $m^{1/2}$. Also, monolithic $MoSi_2$ exhibits hardness of around 10 GPa and fracture toughness of ~3 MPa $m^{1/2}$. The lower hardness (~16.5 GPa) of the developed TiB_2 based composite material is due to second phase ($MoSi_2$) addition and formation of reaction product ($TiSi_2$), both having poor mechanical property. Moreover, observed abnormal grain growth of some TiB_2 grains may also play a role in lowering the hardness. Fig. 4.7 illustrates the propagation of the indentation induced crack. Closer look

at Fig. 4.7 reveals that grey harder TiB_2 particles enhances the crack deflection and the black $TiSi_2$ particle allow crack propagation through it by fracturing. There is also indication of lateral crack generation and crack branching. Crack deflection toughening seems to be the only toughening mechanism. Moreover, the lower toughness of the developed composite may due to the presence of other brittle phases ($MoSi_2$, $TiSi_2$).
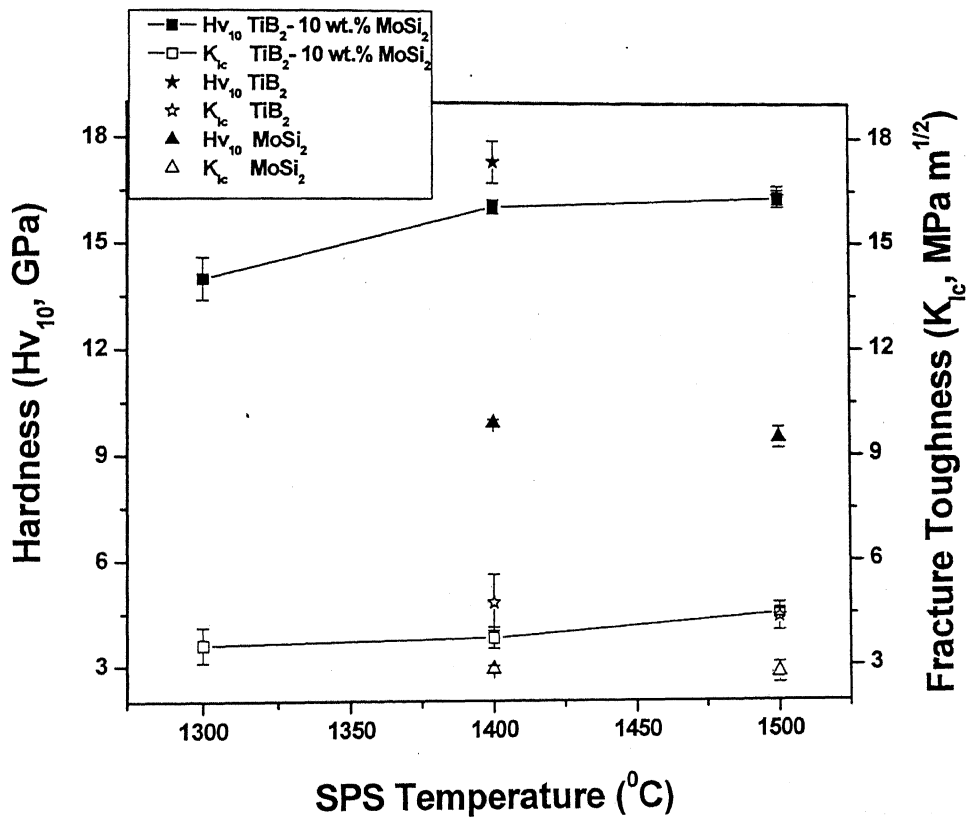

Fig. 4.6. Plot of Vickers Hardness (H_{v10}) and indentation fracture toughness against SPS temperature for TiB_2 -10 wt. % $MoSi_2$ composite, monolithic TiB_2 and $MoSi_2$ ceramics.

The reaction product $TiSi_2$ is characterized by the excellent electrical and thermal property and very poor mechanical properties (bending strength ~ 160 MPa, K_{Ic} ~ 2.2 MPa $m^{1/2}$) [10,11]. Lee et. al synthesized TiB_2-TiN nanocrystalline composite through mechanical activation of the Ti, BN and B powders using ball milling technique followed by plasma sintering to obtain dense composite material. The optimum hardness and fracture toughness exhibited by the TiB_2-TiN are 14.8 to 21.8 GPa and 3.3 to 6.5 MPa $m^{1/2}$ respectively [12]. Reactive hot pressed TiN-TiB_2 composites with 1 wt. % Nickel addition, processed at 1600°C for 30 m, exhibits optimum hardness and fracture toughness of 24 GPa and 6.5 MPa $m^{1/2}$ [13]. Comparison with the literature results this indicate that the addition of $MoSi_2$ and subsequent formation of $TiSi_2$ during SPS sintering restricts the hardness of the composite to around 17 GPa and toughness to ~4 MPa $m^{1/2}$.

Table 4.1 presents the electrical property data of the composite and monolithic materials. The electrical resisitivty values are obtained using the standard four probe method. The electrical resisitivity of the developed composite material increase with increasing SPS processing temperature i.e increases with decrease in porosity and reveals a of 12.38 $\mu\Omega$. cm for composite processed at 1500°C. The electrical resistivity of the monolithic TiB_2 and $MoSi_2$ processed at 1400°C are 13.26 $\mu\Omega$ –cm and 18.87 $\mu\Omega$ –cm respectively. The developed composite exhibits better electrical conductivity value (~0.08-0.09 $M\Omega^{-1}$ .cm^{-1}), when compared with both the monolithic TiB_2 (0.07 $M\Omega^{-1}$ .cm^{-1}) and $MoSi_2$ (0.05 $M\Omega^{-1}$ .cm^{-1}).

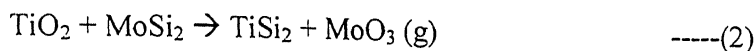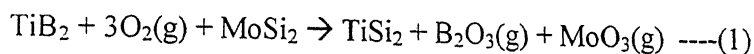*Fig. 4.7. SEM image of crack propagation from the edges of Vickers indentation (H_{v10})*

on TiB₂-MoSi₂ composite (SPS at 1400°C for 10 min) revealing the crack deflection by

grey TiB₂ particle and crack branching.

4.4. Discussion

Apart from low self-diffusion coefficient, additional difficulty in densification of TiB_2 arises from the presence of the surface oxides e.g. TiO_2 and B_2O_3 on particle surface. As far as the present work is concerned, the following issues need to be considered a) role of Spark Plasma sintering in attaining maximum densification at lower sintering temperature and in shorter time, b) role of second phase addition and reaction product on the densification behavior. In SPS process, the densification is assisted by physical and chemical activation of the powder particle surface and this adds to the driving force for the densification. Thermodynamically, the evaporation of B_2O_3 is much more feasible before densification begins and in addition, residual carbon impurity in TiB_2 starting powders enhances B_2O_3 evaporation [14]. Also, the removal of TiO_2 requires high processing temperature and appropriate binder addition. The combination of grain boundary cleaning mechanism contribution from SPS and reaction product formation by the addition of the sintering additives leads to faster densification of the composite. Moreover, the evaporation of material during SPS is strongly dependent on atomic weight, density and sintering temperature [15]. For our composite, the evaporation rate of $MoSi_2$ will be more when compared to TiB_2. The addition of sintering aid also results in the formation of the reaction product of $TiSi_2$, which in turn promotes the densification and enhances electrical property of the developed composite material. It can be noted here that torizuka et. al. studied the densification of TiB_2-ZrO_2 (2Y) with addition of $TiSi_2$ (4 wt.%) at 1700°C under vacuum and reported the attainment of ~94% ρ_{th}. They also indicated the densification enhancement due to the presence of $TiSi_2$ [16].

The thermodynamically feasible reaction leads to the formation of reaction product is as follows,

$$TiB_2 + 3O_2(g) + MoSi_2 \rightarrow TiSi_2 + B_2O_3(g) + MoO_3(g) \quad ----(1)$$

$$TiO_2 + MoSi_2 \rightarrow TiSi_2 + MoO_3 (g) \qquad -----(2)$$

Based on the available data for the free energy of formation of different compounds, it was found that the overall free energy change for reaction (2): $\Delta G_2 > 0$ at high temperature (>1773K). Hence the reaction involving chemical interaction of TiO$_2$ and MoSi$_2$ resulting in the formation of TiSi$_2$ is thermodynamically not feasible. However, the thermodynamic calculations reveal that the overall free energy change for first possible reaction, i.e. $\Delta G_1 < 0$ at and above 1673K (1400°C) ($\Delta G_1 \sim -184.946$ Kcal at 1700K). Hence, the first reaction leading to the formation of TiSi$_2$ is thermodynamically feasible.

The formation of the reaction product provides the active path for the mass transportation during the sintering process. The formation of stable TiSi$_2$ is also reported in literature [17,18]. Sade and Peelleg reported the formation of TiSi$_2$ from the reaction with TiB$_2$ containing free Ti and with Si substrate during annealing above 765°C [17]. TEM analysis of TiB$_2$-20 wt. % MoSi$_2$, hot pressed at 1700°C (1 hr) recently revealed the presence of TiSi$_2$ at the grain boundary triplet [18]. The formation of TiSi$_2$ is also considered to provide as additional diffusion barrier in the microelectronics [11]. This work also revealed the formation reaction product TiSi$_2$ is activated in the presence of SiO$_2$ layer on the substrate. It was observed by Miles et. al. that the presence of small amount of Molybdenum, increases the availability of C54-TiSi$_2$ forming nuclei by order

of two fold [11]. In our case, the presence of $MoSi_2$ particles as second phase provides more stability of the reaction product.

As far as the mechanical properties are concerned, it is observed that the presence of $MoSi_2$ and the formation of $TiSi_2$ restricts the enhancement of hardness and toughness of the composites. $TiSi_2$ is typically characterized by low density, strength retention at high temperature and excellent thermal and electrical conductivity [11-14]. It is also known that the grain size is important in TiB_2-based materials, since the internal stress generation during cooling due to expansion anisotropy generates microcrakcs, if the grain size exceeds the critical limit of 15-20 μm. As the TiB_2 grain size in composite is in the range of ~1-3 μm, the problem of microcracking is avoided in the developed composite. As far as the electrical conductivity is concerned, the presence of high conductivity $MoSi_2$ and $TiSi_2$ phases enhances the electrical property in the composites as compared to TiB_2 monolith.

References:

[1] S. Torizuka, K. Sato, H. Nishio and T. Kishi, "Effect of SiC on interfacial reaction and sintering mechanism of TiB_2", J. Am. Ceram. Soc., 78 [6] 1606-1610 (1995).

[2] S. Tuffe, J. Dubois, G. Fantozzi and G. Barbier, Densification, Microstructure and Mechanical Properties TiB_2-B_4C Based Composites, Int. J. of Refractory Metals and Hard Materials 14 305-310 (1996).

[3] Wang Yucheng and Fu Zhengyi, Study of temperature field in spark plasma sintering, Materials Science and Engineering B90 34 - 37 (2002).

[4] J. R. Groza, A. Zavalianges, Sintering Activation by external electric field, Mat. Sci. and Engg., A287 171-177 (2000).

[5] L-H. Li, H-E. Kim, E.S. Kang, "Sintering and mechanical properties of titanium diboride with aluminum nitride as a sintering aid", J. Eur. Cer. Soc., 22 973-977 (2002).

[6] J. Ho Park, Y. Koh, H. Kim C. Hwang and E. Kong, "Densification and Mechanical Properties of Titanium Diboride with Silicon Nitride as Sintering Aid", J. Am. Ceram. *Soc.,* 82 [11] 3037-3042 (1999).

[7] H. Shimizu, M. Yoshinaka, K. Hirota, O. Yamagunchi, Fabrication and Mechanical properties of monolithic $MoSi_2$ by Spark Plasma Sintering, Mat. Res. Bull, 32 1557-1563 (2002).

[8] Chou TC, Nieh TG, Mechanism of $MoSi_2$ pest during low temperature oxidation, J. Mater. Res. 8 [1] 214 (1993).

[9] Y. Q. Liu, G. Shao, P. Tsakiropoulos, On the Oxidation behaviour of $MoSi_2$, Intermetallics, 9 125-136 (2001).

[10] J Li, D. Jiang, S Tan, Microstructure and mechanical properties of in situ produced $SiC/TiSi_2$ nanocomposites, J. Eur. Ceram. Soc., 20 227-233 (2000).

[11] G. L. Miles, R. W. Mann and J. E. Bertsch, $TiSi_2$ phase transformation characteristics on narrow devices, Thin Solid Film 290-291 469-472 (1996).

[12] J W Lee, Z. A. Munir, M. Shibuya and M. Ohyanagi, Synthesis of Dense TiB_2-TiN Nanocrystalline Composites through Mechanical and Field Activation, J. Am. Ceram. Soc., 84 [6] 1209-1216 (2001).

[13] L. Rangaraj, C. Divakar and V. Jayaram, Reactive Hot pressing of Titanium Nitride-Titanium Diboride Composites at Moderate pressures and temperature, J. Am. Ceram. Soc., 87 [10] 1872-1878 (2004).

[14] S. Baik and P.F. Becher, "Effect of oxygen contamination on densification of TiB_2," *J. Am. Ceram. Soc.*, 70 [8] (1987) 527-30.

[15] R. Holm, Electric contacts: Theory and applications, 4th end Spring, New York, 1967.

[16] S. Torizuka, K. Sato, J. Harada, H. Yamamot and H. Nishio, "Microstructure and sintering mechanism of TiB_2-ZrO_2-SiC composite", J. Ceram. Soc. Japan, 100 [4] 392-397 (1992).

[17] G. Sade and J. Pelleg, Co-Sputtered TiB_2 as a diffusion barrier for advanced microelectronics with Cu metallization, Applied Surface Science, 91 263-268 (1995).

[18] B. Basu, K. Biswas, T.S.R. Ch. Murthy, A.K.Suri and K. Chattopadhya, TEM investigation and densification mechanism of novel TiB_2-based composite (communicated to Scripta Materialia 2004.

Chapter 5

Results and Discussion
-TiB$_2$/Cu Cermet

5. Results and Discussion

5.1 Densification

At the first stage of the present work, the SPS experiments were carried out on TiB_2/Cu system and the SPS parameters were optimized. The densification data of the TiB_2-6 wt. % Cu cermets, Spark Plasma Sintered at various sintering temperature (1200°C-1500°C) and various holding period (10 and 15 min) is presented in Fig 5.1. Fig.5.1 reveals the densification behavior of the TiB_2-6 wt. % Cu composites, indicating that the developed TiB_2 based cermet with maximum density of ~99%ρ_{th} could be obtained after SPS processing at 1500°C for a holding period of 15 min. Initially, the sintering was carried out for TiB_2/Cu cermets for the short holding period of 10 min for varying sintering temperature (1200°C to 1500°C) and the sintered density of more than 90%ρ_{th} was obtained only after SPS processing at 1500°C. In general, the densification behavior exhibits a gradual increase in sintered density with increasing sintering temperature form 1200°C to 1500°C. Subsequently, the densification experiments were conducted with little longer holding period of 15 min at the sintering temperature of 1400°C and 1500°C in order to achieve higher densification. There is a significant densification improvement with increasing the holding period from 10 min to 15 min. The difference in sintered density with holding time is significantly noticed especially at higher sintering temperature of 1500°C.

The results reveals that TiB_2 with lower amount (6 wt.%) sintering additives (Cu) exhibits maximum densification at sintering temperature of 1500°C for a holding period of 15 min. Our recent work showed that ~98%ρ_{th} can be obtained in monolithic TiB_2 after hot pressing at 1800°C for 1 hr [1]. Hence the present experimental results clearly
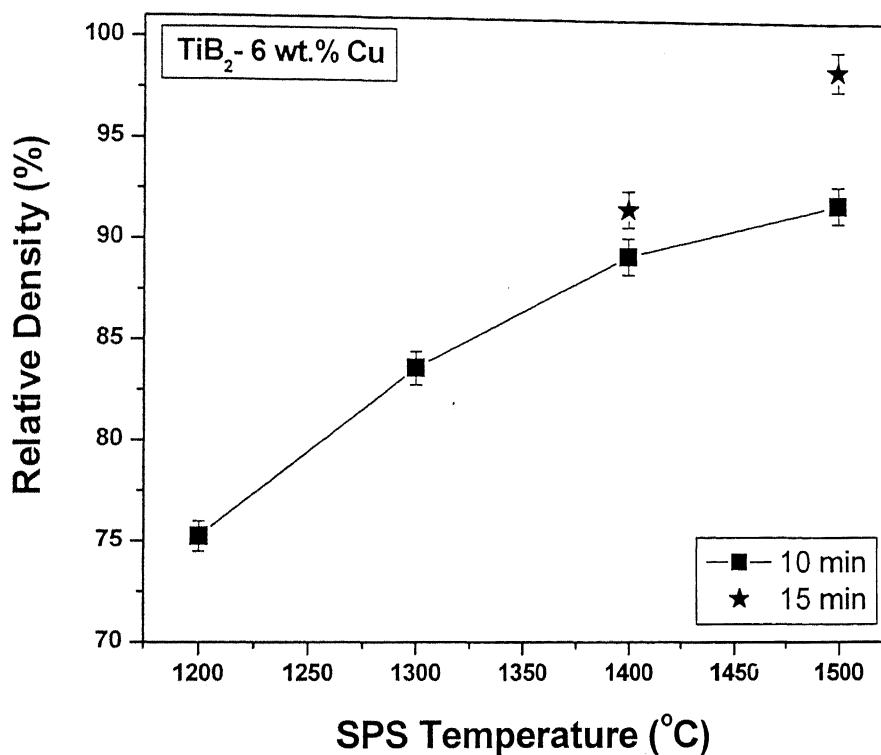
Fig. 5.1. Plot of relative density vs. SPS temperature spark plasma synthesized TiB₂-6 wt. % Cu (a) cermets for various holding time at peak sintering temperature.

indicate that both Cu addition as well as SPS processing enables to achieve high densification much faster at 1500°C for 15 min with a heating rate of 500K/min. To this end, it can also be mentioned that our previous investigation on the TiB_2 based material with ceramic binder ($MoSi_2$) addition, sintered via SPS route, revealed maximum densification (~98% ρ_{th}) at 1400°C [2]. Collectively looking at densification behavior, the grain boundary cleaning effect contribution from SPS and liquid phase sintering (LPS) from Cu together contribute to achieve maximum densification at lower temperature in a shorter time. The LPS and physical activation enhance the kinetics of the sintering and aid in mass transport effectively, which results in better densification. Densification of the TiB_2 – (0.5 wt. %) Fe and Cr cermet was carried out in the temperature range of 1800-1900°C for 2 hr to obtain maximum densification (~98-99%ρ_{th}) [3]. Feber et. al. have used upto 10 wt. % Ni to achieve more than 99% theoretical density in TiB_2 cermets by hot pressing route (~1400°C) [4]. It was reported by Einarsrud and co-workers that the effect of relatively small addition of (1-5 wt. %) of nickel, NiB and iron promotes the liquid phase sintering of TiB_2 [5].

5.2 Microstructure

The cermets selected for detailed microstructure study are the materials, SPSed at 1500°C, for a holding period of 15 min, which exhibits maximum in densification behavior. XRD spectra obtained with the TiB_2 – 6 wt. % Cu cermets are presented in Fig. 5.2, exhibiting the phase analysis of the TiB_2-based cermet, revealing the predominant presence of TiB_2 and metallic Cu. No reaction product is detected within the resolution limit of XRD. There is no indication of formation of any reaction product.
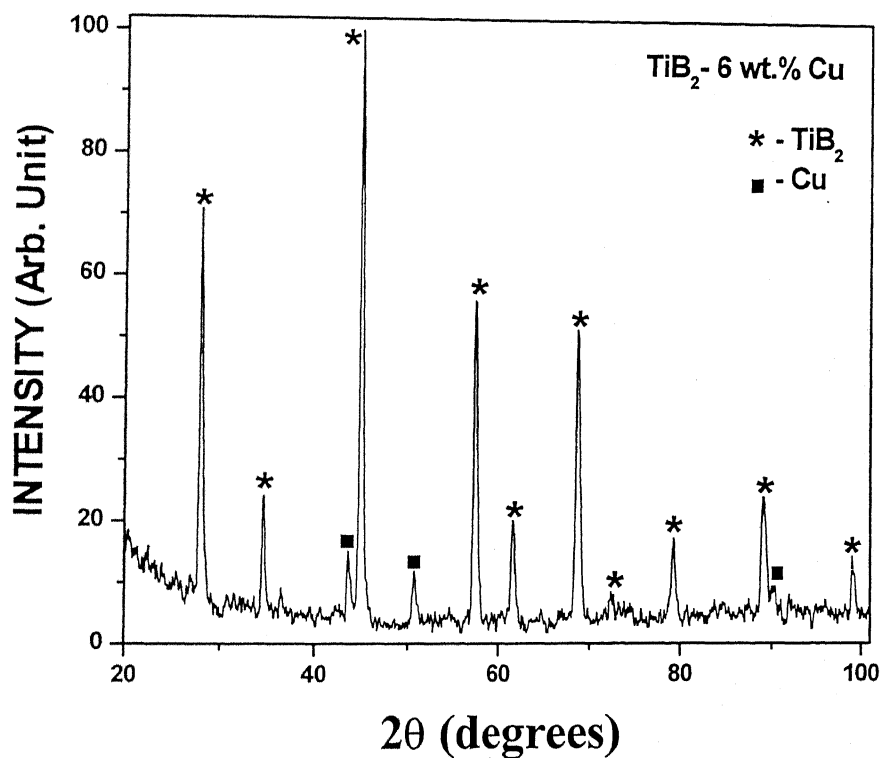
Fig. 5.2. X-ray diffraction pattern of TiB₂- 6 wt. % Cu , SPSed at 1500°C for 15 min under vacuum. The different crystalline phases are mentioned in the inserts of the plot.

SEM micrographs (BSE contrast) of the polished and fractured surface TiB$_2$ – 6 wt. % Cu cermet, SPSed at 1500°C are displayed in Fig.5.3. The fracture surface (Fig. 5.3b) of the TiB$_2$-6 wt. % Cu cermet is characterized by predominantly intergranular fracture mode. On the polished surfaces (Fig. 5.3a), the presence of pores having rounded as well as hexagonal morphology is observed in the TiB$_2$ grains. The TiB$_2$ grain shape in the cermet is of different morphology of faceted, rounded, platelet like. Moreover, the grain size of the TiB$_2$ grains is non-uniform in nature and the observation of finer as well as coarser grains/elongated grains with longer aspect ratio is noted. The microstructure of the TiB$_2$ based cermet is characterized by the presence of three phase i.e black, grey and white. The X-ray mapping analysis is carried out on the selected region of polished TiB$_2$–6 wt. % Cu cermets. Fig. 5.4 shows the corresponding microstructural region along with X-ray intensity distribution of relevant elements (Ti, B, Cu). The X-ray mapping results indicate the predominant presence of Ti and B (black phase), constituent elements of the titanium di-boride. The presence of Cu is much clear around the TiB$_2$ grains and appears as a gray phase. The presence of Cu ensures proper wetting of the TiB$_2$ grains. EDS analysis of the white phase indicate the presence of W, which may incur during the initial ball milling experiments. Overall, the presence of Cu (melting point ~1060°C) helps in the densification of the composite at much lower temperature and enhance the properties of the developed composite material. A closer look at the microstructure reveals the existence of a rim phase with some dissolved Ti and Cu around the TiB$_2$ grains. This dissolution of Cu presumably plays an important role in the shape change of the TiB$_2$ grains. It has been reported by chae et. al that the irregular solid grain is formed due to the dissolution and repricipitation at certain specific grain surfaces [6]. This type of
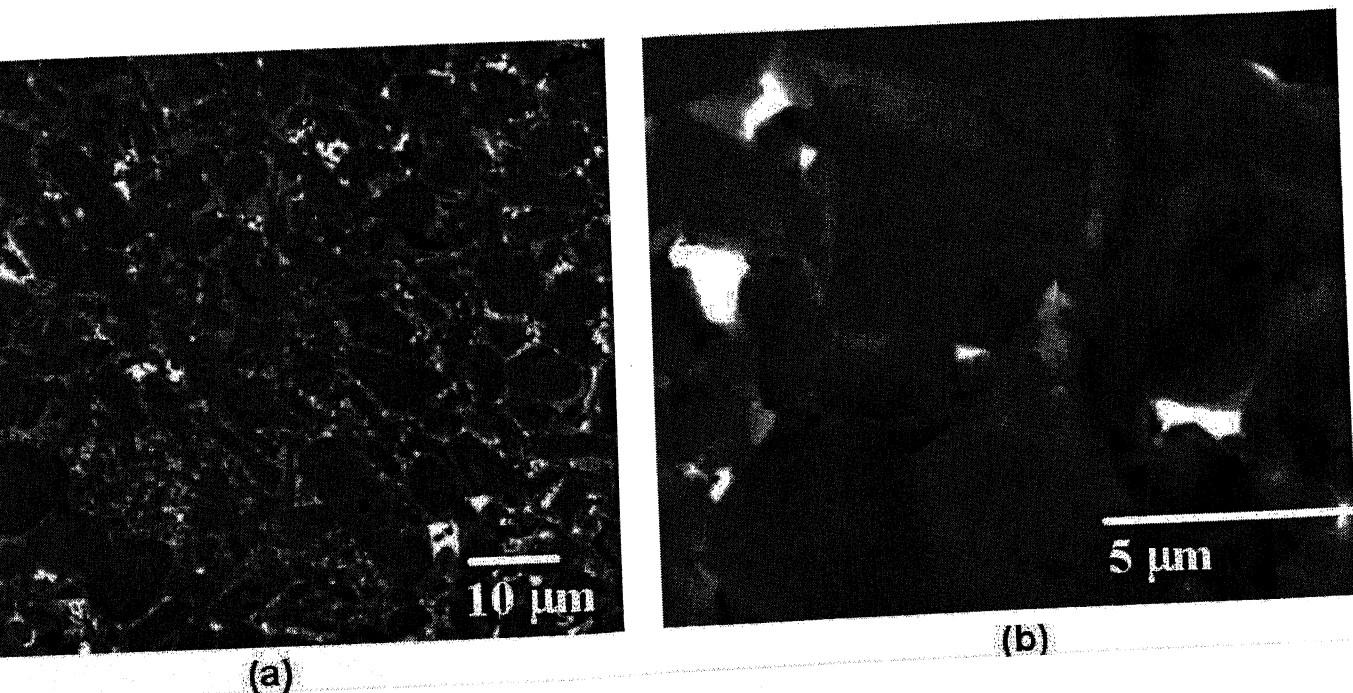
Fig. 5.3. Scanning electron micrographs of polished surface (a) and fracture surface (b) exhibiting different morphology (rounded, elongated, plate like) of TiB$_2$ grains (grey contrast) the TiB$_2$-6 wt. % Cu composite, SPSed at 1500°C for 15 m under vacuum.

Fig. 5.4. X-ray mapping analysis of the TiB₂ -6 wt. % Cu composite, SPSed at 1500°C for 15 min in vacuum. X-ray intensity maps for relevant elements; Ti (b), B(c) and Cu (d) as well as the investigated microstructural region are shown (a) (polished section).

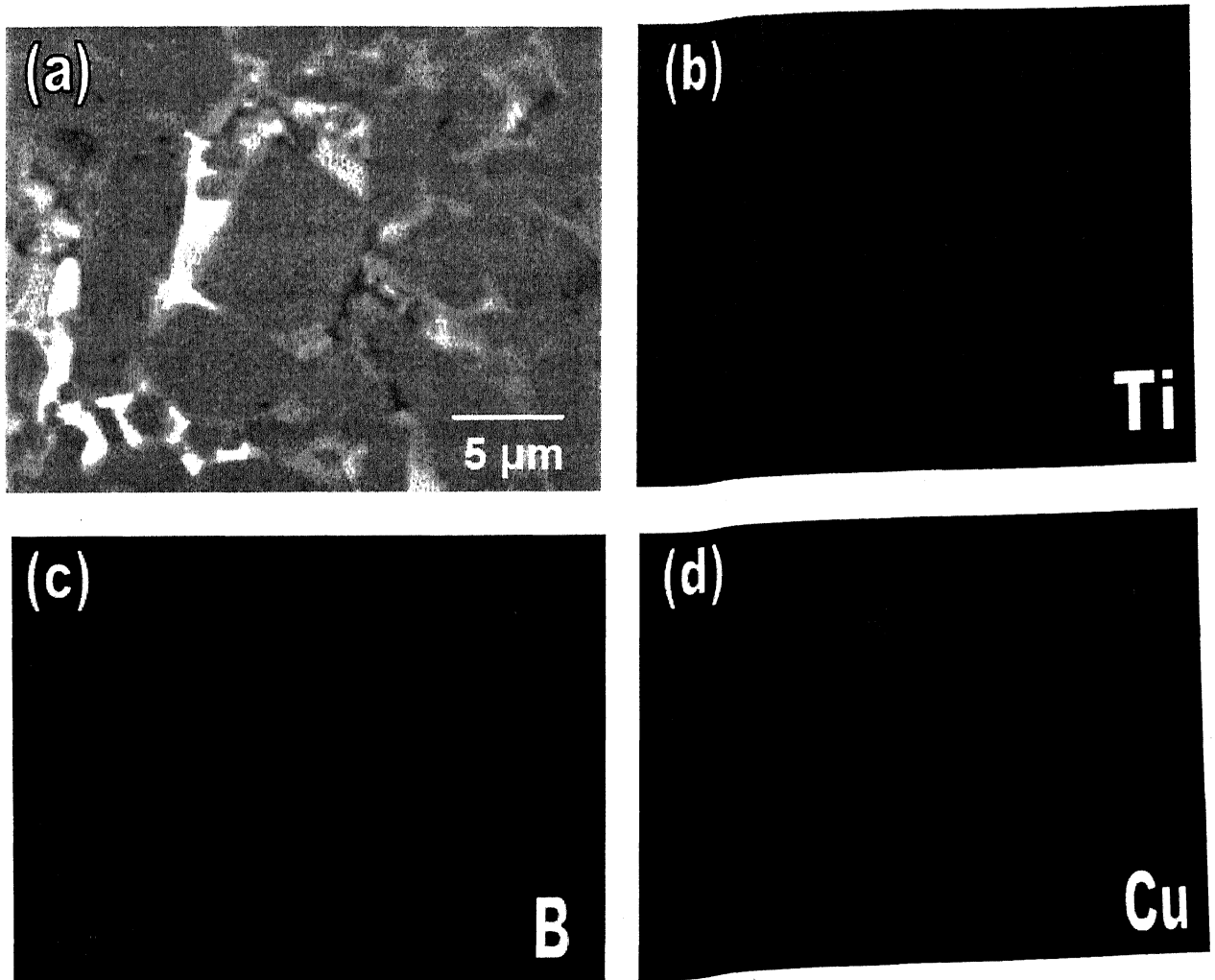grain shape change can be correlated with the tendency towards attaining the equilibrium grain shape or to obtain more stable structure. Han et. al observed the shape change from faceted to spherical of ZnO grains in the presence of the Bi_2O_3 liquid [7]. In the present case, an observation of shape change at higher temperature (1400°C -1500°C) is predominantly observed with the cermet sintered for longer holding time of 15 min. Based on the above observations, it can be started that Ti from borides dissolve in the liquid Cu phase and repricipitation of (Ti, Cu) solid solution takes place on TiB_2 particles during SPS process. The dissolution-precipitation process, being dependent on starting particle shape and size, occurs with varying severity, as also observed in our materials. The presence of a characteristic core-rim structure, with a rim phase having different electron contrast, can be critically made. Similar core-rim structure is widely reported for various ceramic materials like Y-TZP [8] as well as cermet materials like TiCN-Ni [9] etc.

5.3 Mechanical and Electrical Properties

Table 5.1 presents the mechanical properties of the developed TiB_2 based cermets, SPSed at 1500°C for a holding period of 15 m under vacuum. The TiB_2-6 wt. % Cu exhibits optimum hardness and fracture toughness of ~17 GPa and ~11 MPa m$^{1/2}$ respectively. The fracture toughness of the cermet is almost double than that of the monolithic TiB_2 (~4-5 MPa m$^{1/2}$), hot pressed at 1800°C for 1 hr [10]. It can also be noted that the TiB_2 based cermet with 0.5 wt. % Fe and Cr addition, pressureless sintered at 1800°C exhibits strength of 506 MPa and fracture toughness of 6.6 MPa. m$^{1/2}$ [3]. TiB_2 with 1.4 wt. % Ni, hot pressed at 1400°C exhibits hardness and fracture toughness of 670 MPa and 6.4 MPa m$^{1/2}$ respectively. Addition of Ni more than 2 wt. % to TiB_2 results in the formation

Table.5.1 Mechanical and electrical properties of the developed TiB$_2$-6 wt.% Cu cermet,

SPSed at 1500°C for 15 min under vacuum.

Material	Density (gm/cc)	Relative Density (ρ_{th}, %)	Vickers Hardness (Hv10, GPa)	Fracture Toughness (K_{Ic}, MPa m$^{1/2}$)	Electrical Resistivity (ρ, $\mu\Omega$-cm)	Electrical conductivity (ρ, MΩ^{-1}-cm^{-1})
TiB$_2$ – 6 wt.% Cu	4.715	98.58	16.7±2.5	10.9±1.7	4.9	0.20

of brittle grain boundary phase, which in turn degrades the properties [4]. From the above, it is clear that the fracture toughness of the newly developed cermets are much higher than earlier developed cermets. However, the addition of softer phase like Cu does not seem to degrade the hardness as similar hardness of 17 GPa is measured in both monolithic TiB_2 and SPS processed TiB_2-6 wt. % Cu cermet.

The obtainment of higher toughness in the newly developed cermets requires some discussion. In the case of monolithic TiB_2, the contribution to toughness arises primarily from crack deflection. Whereas in case of cermets, the ductile metal bridging contribution to crack closure is observed to significantly enhance the fracture toughness. When a crack propagates in boride cermets, the crack gets deflected by the coarser boride particles. Also, the metallic binder phase (Cu) plastically flows around the crack tip of a propagating crack. Both these factors contribute together to achieve higher toughness in the newly developed cermets. It can be mentioned here that similar mechanism also contributes to enhanced toughness (~13-14 MPa m$^{1/2}$) of WC-6 wt. % Co cermets [11].

Apart from the mechanical properties, the electrical resistivities of the optimized cermets are measured at room temperature using conventional four probe method. The developed materials i.e. TiB_2 based cermets exhibit low resisitivity of ~5 μΩ. cm and high electrical conductivity of 0.20 MΩ^{-1}. cm^{-1} respectively. The TiB_2 based materials exhibits better conductivity, because of less porosity and better interconnected network of metallic binder phase. It can be noted here that the electrical resistivity of pure TiB_2 is 10-30 μΩ-cm The electrical resisitivity of the Cu-48 vol. % TiB_2 composite developed by Yin et.al. exhibits ~ 3.4 μΩ-cm [12]. The electrical resisitivity of the recently developed TiB_2 and TiB_2-10 wt. % $MoSi_2$ composite exhibits in the range of 13.2 μΩ-cm and 12.5 μΩ-cm

respectively [2]. From the above discussion, it should be evident that the addition of smaller amount of Cu in the present case significantly increases the electrical properties of the borides.

The fabrication of transition metal borides based cermets, resembling the well-known WC-Co hard metal, combines the high toughness and electrical conductivity of a metallic binder with the hardness of the boride phase. The experimental results of the present work reveals that, the combination of better mechanical properties and electrical properties can be achieved in TiB$_2$-based cermet and this can be used as a candidate material for various structural applications, especially as electro discharge machining (EDM) electrodes. The electro-conductive toughened ceramics can be shaped by EDM to manufacture complex components, thereby could potentially the number of industrial applications of these materials.

5.4. Reference

[1] T. S. R. Ch. Murthy, B. Basu, R. Balasubramaniam, A. K. Suri, C. Subramanian and R. K. Fotedar, Processing and properties of Novel TiB_2-based composites, communicated to J. Am. Cer. Soc. August 2004.

[2] T. Venkateswaran, B. Basu, DY Kim, "Spark Plasma Sintering of TiB_2-based composite materials", communicated to J. Am. Cer. Soc Dec 2004.

[3] S. Kang and D.J. Kim, E.S. Kang and S. S. Baek, "Pressureless Sintering and properties of Titanium Diboride Ceramics containing Chromium and Iron," *J.Am.Cer.Soc,* 84[4] 893-95 (2001).

[4] M.K. Ferber, P.F. Becher, and C.B. Finch, "Effect of Microstructure on the properties of TiB_2 ceramics," Communications of the American Ceramic Society, January 1983, C2 - C3.

[5] M. Einarsrud, E. Hagen, G. Petterson and T. Grande, "Pressureless Sintering of Titanium diboride with Nickel, Nickel boribe and iron additives", J. Am. Ceram. Soc., 80 [12] 3013-3020 (1997).

[6] KW Chae, DI Chun and DY Kim, "Microstructural Evolution during the infiltration treatment of Titanium Carbide-Iron Composite", J. Am. Ceram. Soc., 73 [7] 1979-82 (1990).

[7] J-H Han, Y-K Chung, D-H Kim, S-H Cho and D. K. Yoon, Temperature dependence of the shape of Zno grains in a liquid matrix, Acta Metall. 37 [10] 2705-2708 (1989).

[8] JJ Kim, C Park and DY Kim," Discontinuous Coarsening of tetragonal Precipitates in Partially Stabilized Zirconia Induced by Diffusional Coherency Strain under Applied Stress", J. Am. Ceram. Soc., 73 [12] 3658-62 (1990).

[9] D. Sarkar, S.Ahn, S.Kang and B. Basu, Fretting Wear of TiCN-Ni cermet: Influence of secondary carbide content, P/M Science and Technology Briefs, 5 [2] 5-11 (2003).

[10] B. Basu, J. H. Lee and D. Y. Kim, "Development of Nanocrystalline wear resistant Y-TZP ceramics", J. Am. Cer. Soc., 87 [9] 1771-1774 (2004).

[11] B. Basu, Jong-Heun Lee and Doh-Yeon Kim, Development of $WC-ZrO_2$ Nanocomposites by Spark Plasma Sintering, J. Am. Cer. Soc., 87 [2] 317-319 (2004).

[12] P Yin, DDL Chung, "Titanium diboride copper-matrix composite", J. Mat. Sci, 32 1703-1709 (1997).

Chapter 6

Conclusions

6. Conclusion

In the present work, the experimental results obtained while developing TiB_2 materials using Cu and $MoSi_2$ as binder is reported. The specific conclusions include:

a) For the first time, binderless densification of monolithic TiB_2 to near theoretical density (~98 % ρ_{th}) is achieved by Spark Plasma Sintering at 1400°C for 10 minutes. The obtained material is characterized by 2-5 μm grain size, high hardness of ~18 GPa and moderate indentation toughness of ~ 5 MPa m$^{1/2}$.

b) Almost fully dense composites are obtained under the same SPS conditions for matrix densification XRD as well as SEM-EDS analysis reveals the formation of $TiSi_2$ phase dispersed in the microstructure. The densification mechanism is dominated by liquid phase sintering in the presence of $TiSi_2$.

c) The improvement of mechanical properties in composite is not considerable as same hardness (~17 GPa) as TiB_2 monolithic is measured. The fracture toughness remains moderate (~ 4.5 MPa m$^{1/2}$) and this is due to the presence of brittle intermetallic phase ($TiSi_2$ and $MoSi_2$). TiB_2 particles size in the composite varies around 1-3 μm.

d) An interesting observation in that high hardness could not be achieved in SPS processed TiB_2-10 wt. % $MoSi_2$ materials, while hot pressing results [1] indicates that more than 20 GPa can be achieved in TiB_2-10 wt. % $MoSi_2$ composites. This could be attributed to the observed grain growth of TiB_2 particles during Spark Plasma Sintering.

It also implicates that the SPS processing needs to be tuned in order to present grain growth of conductive ceramics, like TiB$_2$

e) Although, enhancement of mechanical property is not realized as compared to monolithic TiB$_2$, higher electrical conductivity (0.081-0.092 x 10^6 Ω^{-1} cm^{-1}) is measured with TiB$_2$-10 wt. % MoSi$_2$ composite. This is presumably due to the presence of TiSi$_2$ reaction product.

f) The influence of 6 wt. % Cu addition on the densification of TiB$_2$ is also studied using SPS as a processing tool. The TiB$_2$-6 wt. % Cu cermet was optimally densified to ~99% ρ_{th} 1500°C with holding time of 15 minutes.

g) The sintered microstructure is characterized by a core-rim structure with small amount of Cu dissolved in boride rich rim phase. Ti from boride particles also were found to dissolve in metallic binder phase during the SPS processing. Another characteristic microstructural feature is the change of grain shape from equiaxed to more rounded, which presumably is due to the dissolution-repricipitation phenomenon inherent in liquid phase sintering.

h) The optimum TiB$_2$ cermet exhibits high hardness and fracture toughness of 17 GPa and 11 MPa m$^{1/2}$ respectively. Also, the addition of 6 wt. % Cu leads to enhanced electrical conductivity in TiB$_2$-based cermets (0.20 MΩ^{-1}. cm^{-1}).

i) High toughness in cermet vis-à-vis $TiB_2/MoSi_2$ composite in primarily due to the difference in toughening mechanism. While the crack deflection in the role of toughening mechanism in ceramic composites, the ductile metal bridging additionally contributes to more toughness in the cermet materials.

Reference:

T. S. R. Ch. Murthy, B. Basu, R. Balasubramaniam, A. K. Suri, C. Subramanian and R. K. Fotedar, Processing and properties of Novel TiB_2-based composites (communicated to J. Am. Cer. Soc. August 2004).